*Supporting information*

# Linkage engineering regulated π-conjugated covalent organic frameworks (COFs)-based anode for high-performance LIBs

Changyu Weng[1], Hongmei Yuan[1], Jie Wang[1], Longlong Ma[1,2], Jianguo Liu[1*]

[1] Key Laboratory of Energy Thermal Conversion and Control of Ministry of Education, School of Energy and Environment, Southeast University, Nanjing 210096, PR China.

[2] Department of Thermal Science and Energy Engineering, University of Science and Technology of China, Hefei 230026, P.R. China.

* Corresponding authors' e-mail: liujg@seu.edu.cn

## Contents

## 1. Experimental section

### Materials

All reagents were obtained from commercial supplies and used as received. N-methylpyrrolidone (99.0%), 1,3,5-trimethylbenzene (99.0%), benzimidazole (99.0%), 1,3,5-triformylbenzene (TFB, 99.0%), 2,5-diaminohydroquinone dihydrochloride (DABD, 98.0%), benzene-1,3,5-triamine trihydrochloride (TAB, 98.0%), 2,5-dihydroxyterephthalaldehyde (DHA, 98.0%), 1,4-dioxane (99.5%), acetic acid

(99.0%), tetrahydrofuran (THF, 99.5%), and methanol (99.9%), carbon nanotubes (CNT, purity:>95 wt%, OD:<2nm, length:5-30 μm) were purchased from Tansoole. The acetone (99.0%) was purchased from Sinopharm Chemical Reagent Limited Corporation. Acetylene black and polyvinylidene fluoride (PVDF) were purchased from Canrd.

**Material Characterization**

The synthesis of the samples was verified using Fourier transform infrared spectroscopy (FT-IR, Nicolet IS50, Thermo Fisher Scientific). The crystalline structure of the samples was studied using X-ray diffractometry (XRD, Smartlab (3), Rigaku). The microstructure was investigated using a scanning electron microscope (SEM, Nova Nano SEM450, FEI) and transmission electron microscope (TEM, Talos F200X, Thermo Fisher Scientific). The system of Thermo Scientific K-Alpha was employed to obtain X-ray photoelectron spectroscopy (XPS) spectra. The values of binding energy were calibrated by using C 1s peak at 284.8 eV. Nitrogen adsorption and desorption isotherms were measured at 77 K using a Micromeritics 3Flex. The samples were degassed at 120 °C for 10 h before the measurements. Surface areas were calculated from the adsorption data using Brunauer-Emmett-Teller (BET). Thermogravimetric analysis (TGA) was carried out on TG209 F3 by heating samples from 30 to 900 °C in a dynamic nitrogen atmosphere with a heating rate of 10 °C·min$^{-1}$. the $^{13}$C cross-polarization solid-state nuclear magnetic resonance ($^{13}$C CP/MS NMR) spectrum was performed by Bruker-500. The elemental analysis was studied using a Vairo EL cube. The electrical conductivity was measured by four-probe conductivity measurements (ST2742-B) and high resistance meter measurements (ST2643) under a pressure of 20 MPa.

**Bragg's Law:[1]**

$$n\lambda = 2d\sin\theta$$

where n is the diffraction order (usually n=1), θ is measured from the surface normal, the wavelength λ (Cu Kα : λ=0.15406 nm), and d is the layer spacing of the COFs.

**Density functional theory (DFT) calculation**

The theoretical calculations were based on the DFT using the CASTEP, Dmol3,

and Reflex tools modules of Materials Studio (MS) software. The functional of CASTEP was chosen as Perdew-BurkeErnzerh (PBE) in generalized gradient approximation (GGA).

**The weight ratio of COFs and CNT in COFs@CNT**

The weight ratio of COFs and CNT in the COFs@CNT was investigated based on the N and C contents in the pristine COFs, the CNT, and the COFs@CNT, as shown in Table S1. The two equations can be described as follows:

$$P_{COFs} \times N_{COFs} + P_{CNT} \times N_{CNT} = N_{COFs@CNT}$$
$$P_{COFs} \times C_{COFs} + P_{CNT} \times C_{CNT} = C_{COFs@CNT}$$

Where $N_{COFs}$ and $C_{COFs}$, $N_{CNT}$ and $C_{CNT}$, $N_{COFs@CNT}$ and $C_{COFs@CNT}$ correspond to the weight percentages of N and C in pristine COFs, pristine CNT and the COFs@CNT composite, respectively. $P_{COFs}$ and $P_{CNT}$ correspond to the mass percentages of COFs and CNT in the COFs@CNT composite.

**Capacity contribution of COFs in COFs@CNT calculation**

The composite capacity of COFs@CNT can be regarded as the contribution of two components, as described by the following equation:

$$C_{COFs@CNT} = C_{COFs} \times P_{COFs} + C_{CNT} \times P_{CNT}$$

where $C_{COFs@CNT}$, $C_{COFs}$, and $C_{CNT}$ represent the capacities of COFs@CNT, COFs, and CNT, respectively. $P_{COFs}$ and $P_{CNT}$ correspond to the mass percent of COFs and CNT in the COFs@CNT composite.

## 2. Procedures for COFs Synthesis

**Synthesis of COFs@BOA**
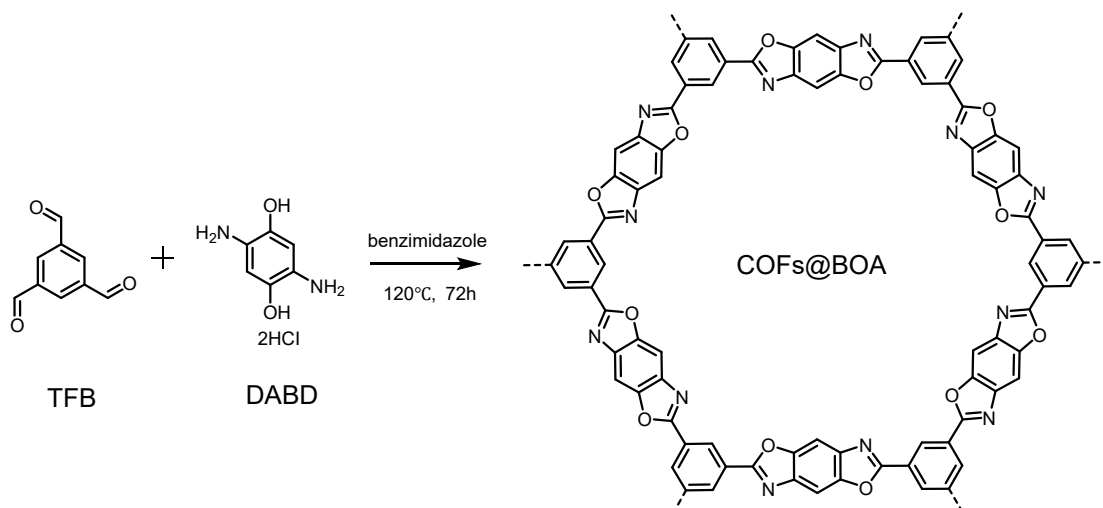
TFB (48.6 mg, 0.3 mmol) and DABD (95.8 mg, 0.45 mmol) were suspended in a mixture of *N*-methylpyrrolidone and 1,3,5-trimethylbenzene (1:1 V: V, 5 mL). After the mixture was sonicated for 20 min, benzimidazole (159.5 mg, 1.35 mmol) was added. Subsequently, the Pyrex tube was frozen at 77 K using a liquid $N_2$ bath and degassed by three freeze-pump-thaw cycles, then sealed under vacuum and heated at 120 °C for 72 hours. The resulting COFs@BOA precipitate was isolated by vacuum filtration and washed with THF, methanol, and acetone, then dried at 100 °C under vacuum for 24 hours to give the desired COFs@BOA.

### Synthesis of COFs@BOA-30 and COFs@BOA-15

The COFs@BOA-30 and COFs@BOA-15 were prepared using a similar synthesis method. The only difference was that the CNT (COFs@BOA-30: 43.3 mg; COFs@BOA-15: 21.7 mg) was added at the same time as TFB (48.6 mg, 0.3 mmol) and DABD (95.8 mg, 0.45 mmol). The other processes were consistent with those used to prepare COFs@BOA.

### Synthesis of COFs@IM
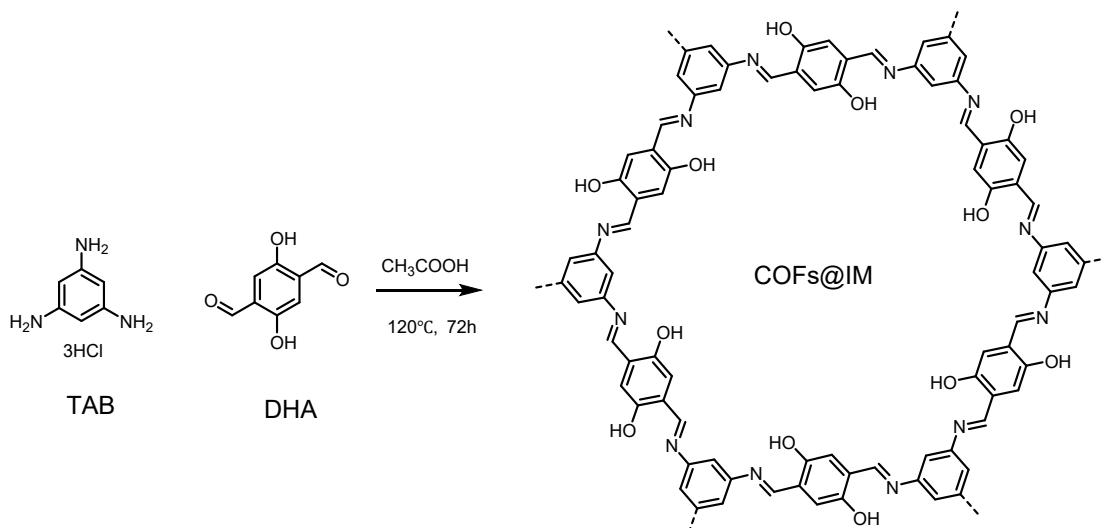
TAB (69.7 mg, 0.3 mmol) and DHA (74.7 mg, 0.45 mmol) were suspended in a mixture of mesitylene and dioxane (1:1 V: V, 2 mL). After the mixture was sonicated for 20 minutes, acetic acid (6 M, 0.2 ml) was added. Subsequently, the Pyrex tube was frozen at 77 K using a liquid $N_2$ bath and degassed by three freeze-pump-thaw cycles, then sealed under vacuum and heated at 120 °C for 72 hours. The resulting COFs@IM precipitate was isolated by vacuum filtration and washed with THF, methanol, and acetone, then dried at 100 °C under vacuum for 24 hours to give the desired COFs@IM.

**Synthesis of COFs@IM-30 and COFs@IM-15**

A similar synthesis method was applied to prepare the COFs@IM-30 and COFs@IM-15. The only difference was that adding the CNT (COFs@IM-30: 43.3 mg; COFs@IM-15: 21.7 mg) at the same times as adding TAB (69.7 mg, 0.3 mmol) and DHA (74.7 mg, 0.45 mmol). Other processes were consistent with the preparation of COFs@IM.

**Synthesis of COFs@BOA/30 and COFs@IM/30**

COFs@BOA/30 and COFs@IM/30 were synthesized through a simple physical mixing technique. The COFs@BOA with 70 mg (COFs@IM with 46 mg) and CNT with 30 mg (54 mg) were transferred to a mortar and then ground for a 30 min grind to obtain homogeneous composites.

## 3. Electrochemical measurements

Coin-type (CR2032) cells were assembled in an Ar-filled glove box ($H_2O < 0.1$ ppm, $O_2 < 0.1$ ppm) with lithium metal foil as the anode and Celgard 2325 as the separator. The electrolyte was 1.0 M $LiPF_6$ in a mixture of dimethyl carbonate (DMC) and ethylene carbonate (EC) (1:1 v/v). The active materials (COFs and COFs@CNT

were treated by ball milling for 8 hours) were mixed with acetylene black and polyvinylidene fluoride binder (PVDF) solution in a weight ratio of 6:3:1 in *N*-methyl-2-pyrrolidinone (NMP) respectively. The slurry was cast on the Cu foil and dried for 10 h at 100 °C under vacuum to remove NMP. The discharge and charge measurements were carried out on a Land instruments CT3001A testing system at various current densities of 100-2,000 mA g$^{-1}$ with a cut-off voltage of 0.005-3.0 V vs Li$^+$/Li. Cyclic voltammetry (CV) and electrochemical impedance spectroscopy (EIS) measurements were conducted using the coin cells on a CHI 760E electrochemical workstation.

# 4. Elemental analysis

Table S1 Elemental analysis results of pristine COFs, CNTs, and COFs@CNT

| Samples | N (%) | C (%) | H (%) |
|---|---|---|---|
| COFs@BOA | 11.818 | 62.225 | 5.164 |
| COFs@BOA-30 | 9.455 | 69.696 | 5.137 |
| COFs@IM | 8.697 | 61.887 | 6.097 |
| COFs@IM-30 | 5.740 | 70.384 | 5.100 |
| CNT | 3.701 | 84.173 | 4.112 |

# 5. X-ray diffraction (XRD)
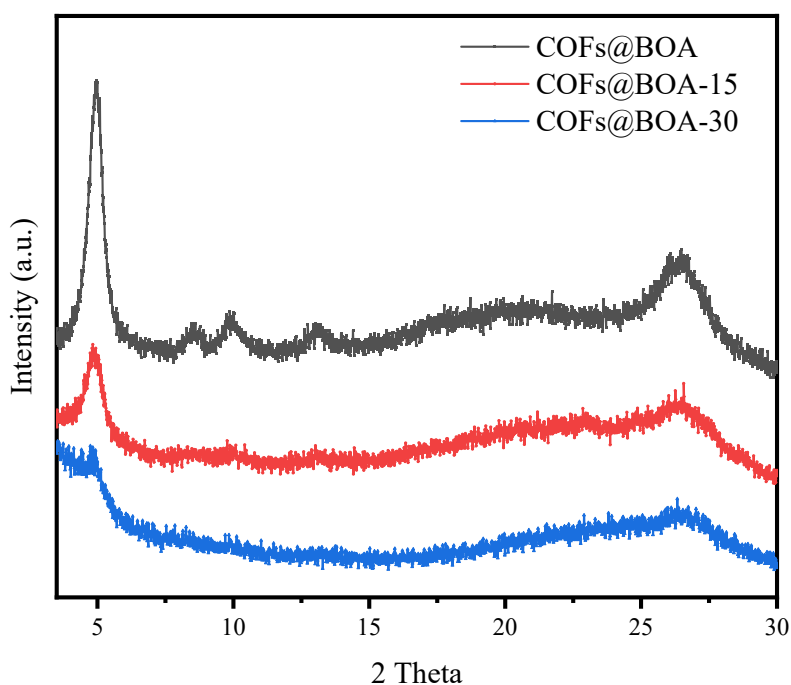


**Fig. S1** XRD patterns of COFs@BOA, COFs@BOA-15, and COFs@BOA-30.
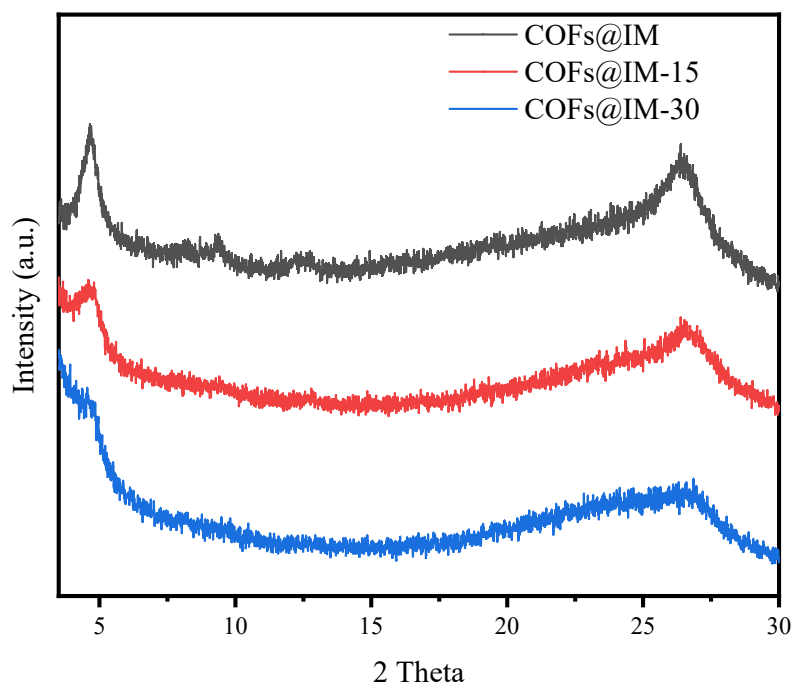
**Fig. S2** XRD patterns of COFs@IM, COFs@IM-15, and COFs@IM-30.
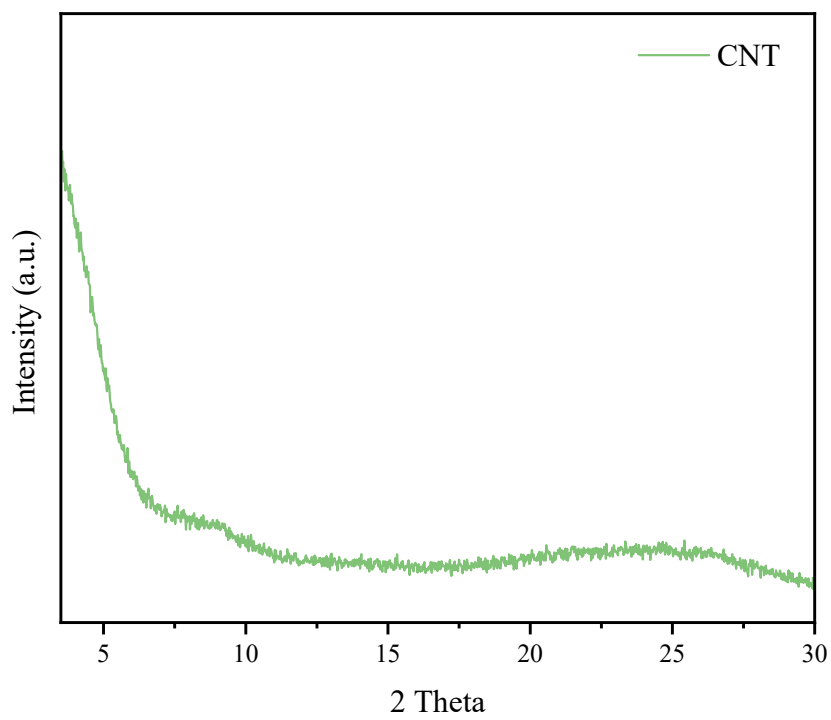


**Fig. S3** XRD patterns of pure CNT.

## 6. Nitrogen adsorption-desorption isotherms

**Table S2.** Structural properties of COFs, COFs@CNT composite, and CNT calculated based on nitrogen adsorption analysis.

| Sample name | BET (m²/g) |
|---|---|
| COFs@BOA | 809 |
| COFs@BOA-30 | 445 |
| COFs@IM | 57 |
| COFs@IM-30 | 155 |
| CNT | 1,300 |
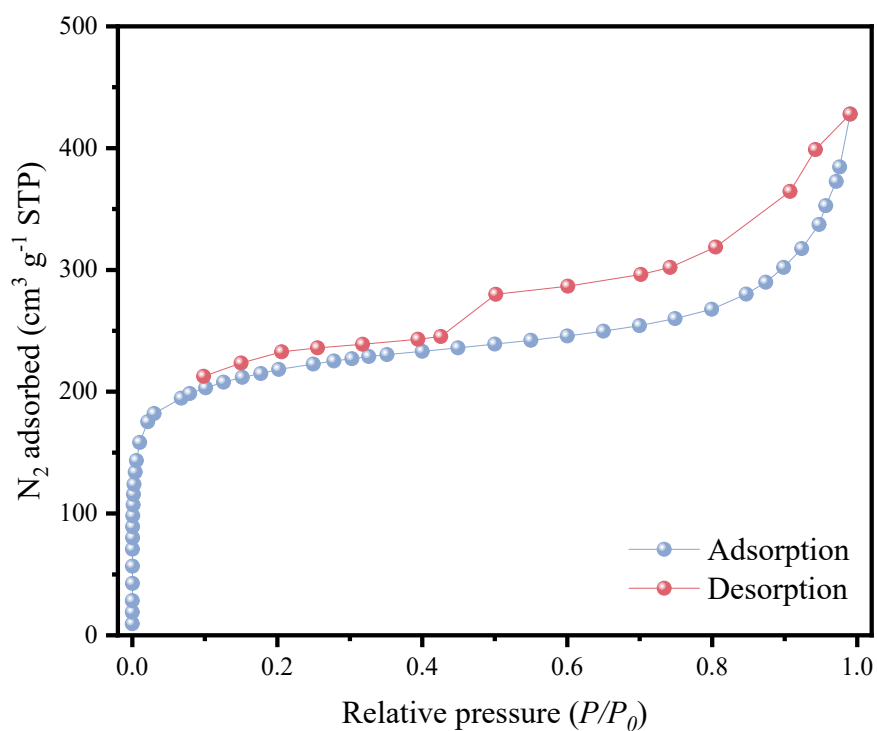


**Fig. S4** Nitrogen adsorption-desorption isotherms of COFs@BOA.
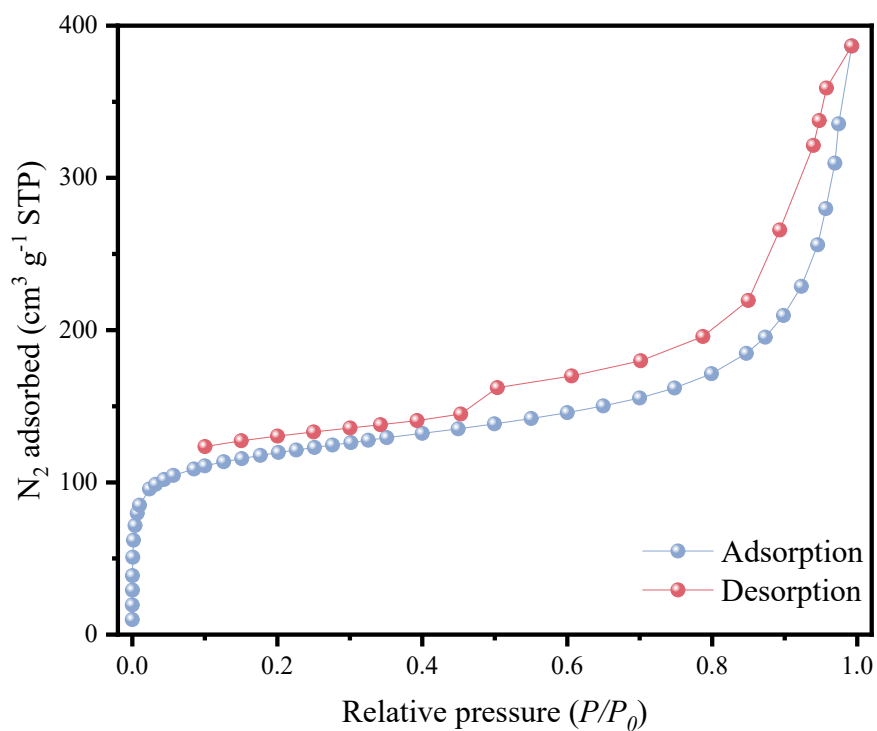
**Fig. S5** Nitrogen adsorption-desorption isotherms of COFs@BOA-30.
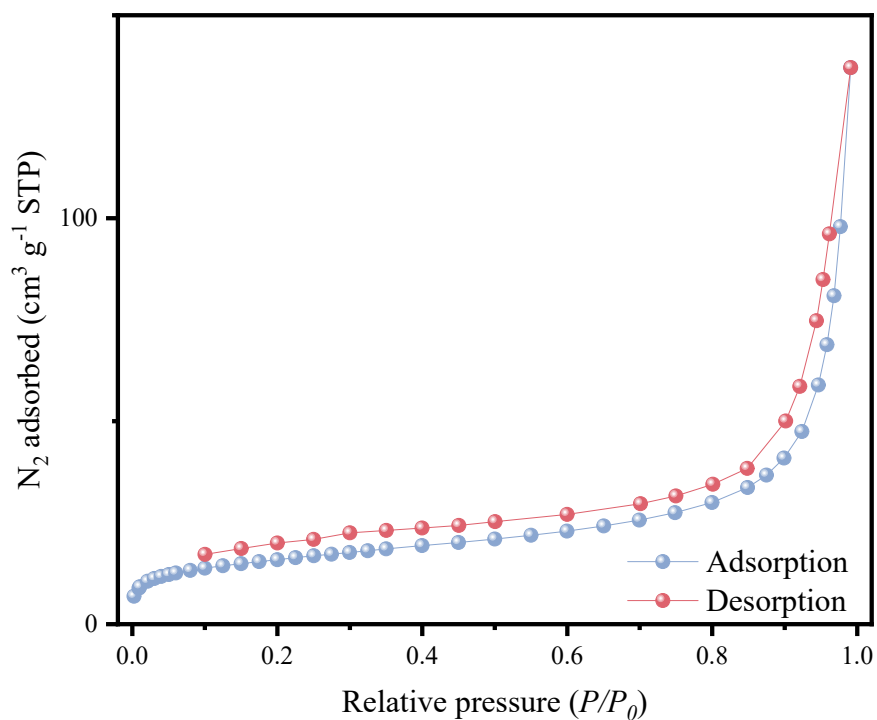


**Fig. S6** Nitrogen adsorption-desorption isotherms of COFs@IM.
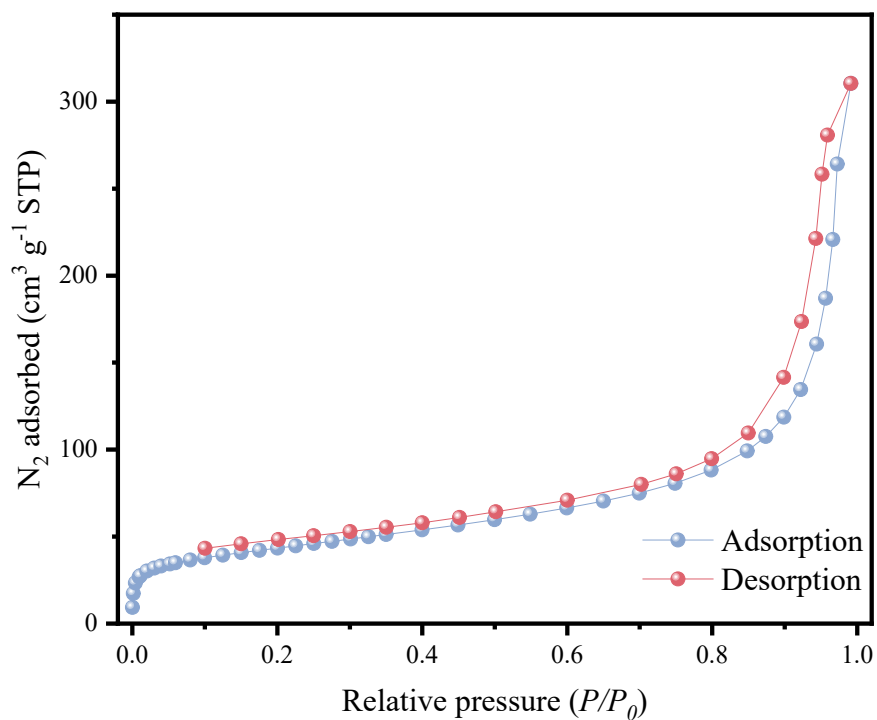
**Fig. S7** Nitrogen adsorption-desorption isotherms of COFs@IM-30.
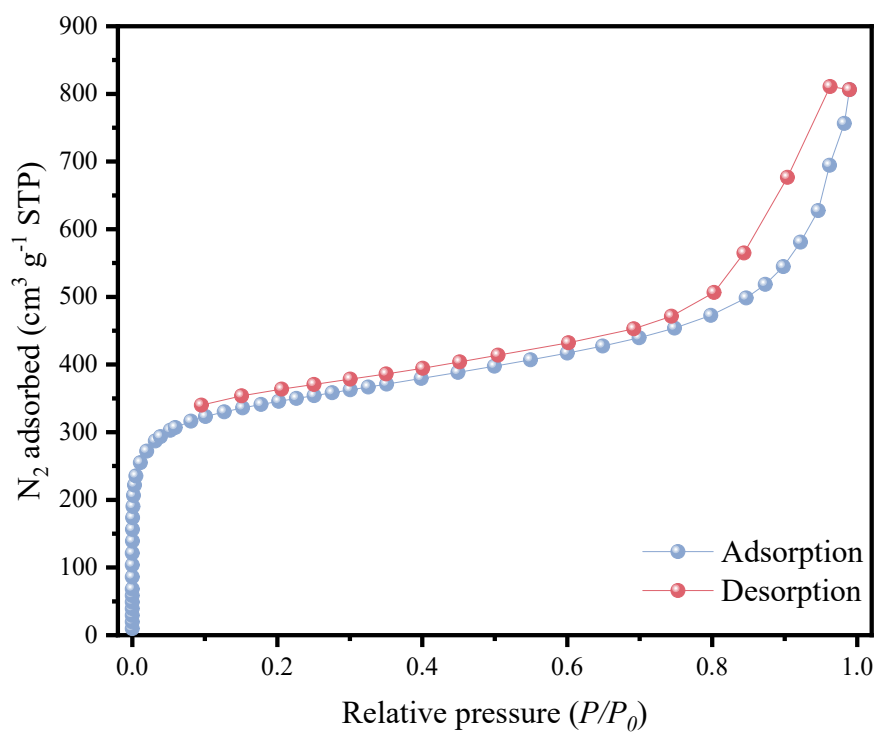


**Fig. S8** Nitrogen adsorption-desorption isotherms of CNT.

# 7. Thermal Gravimetric Analysis
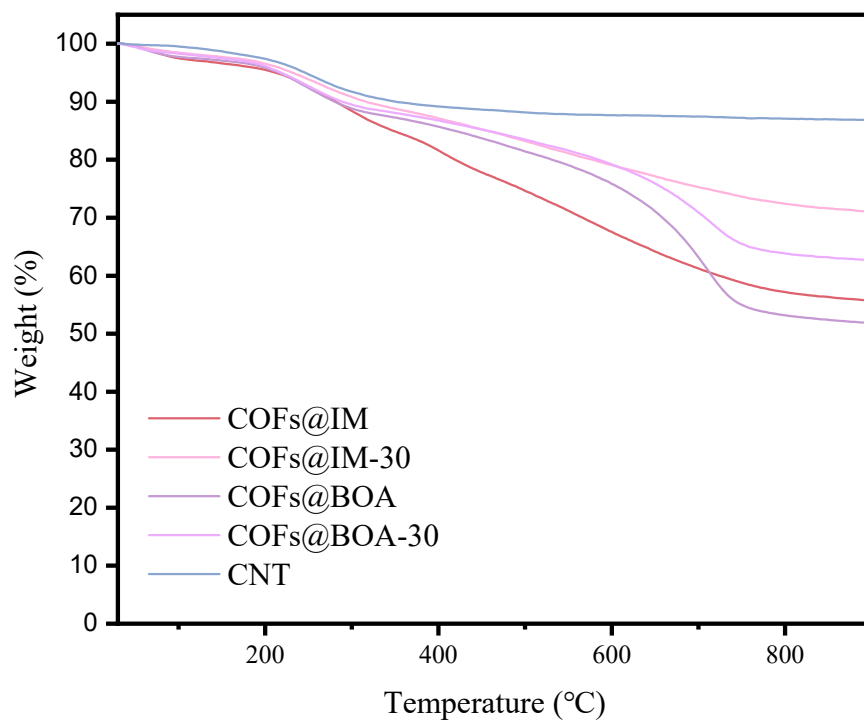


**Fig. S9** The TGA curves of COFs@IM, COFs@IM-30, COFs@BOA, COFs@BOA-30, and CNT.

## 8. Scanning Electron Microscope
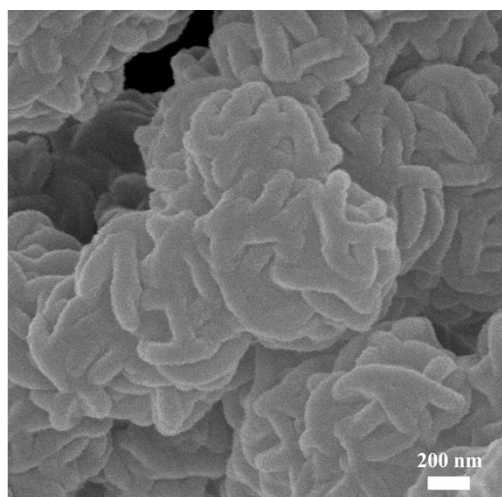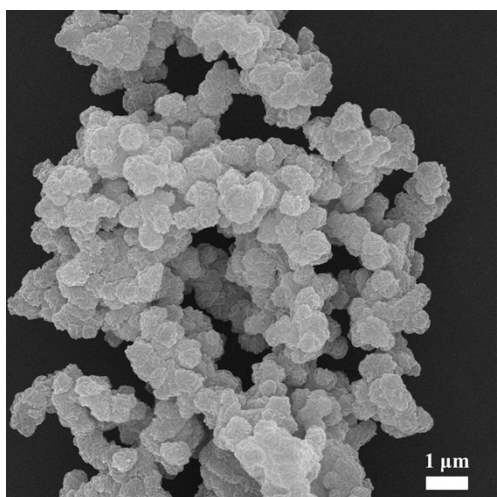
**Fig. S10** SEM images of COFs@BOA
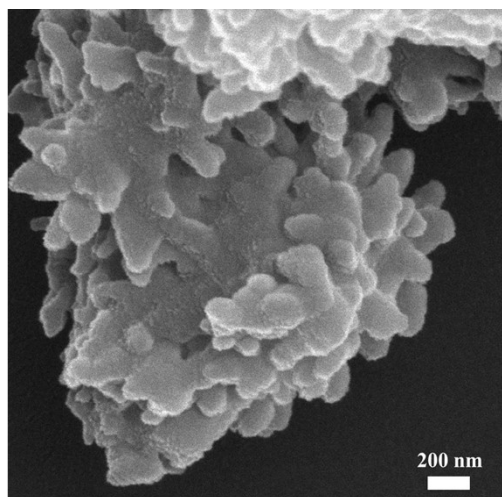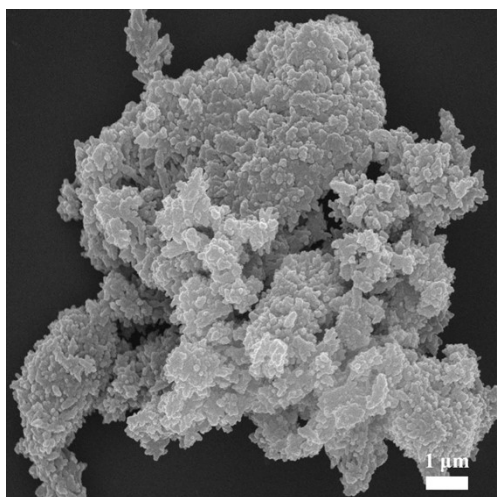


**Fig. S11** SEM images of COFs@IM
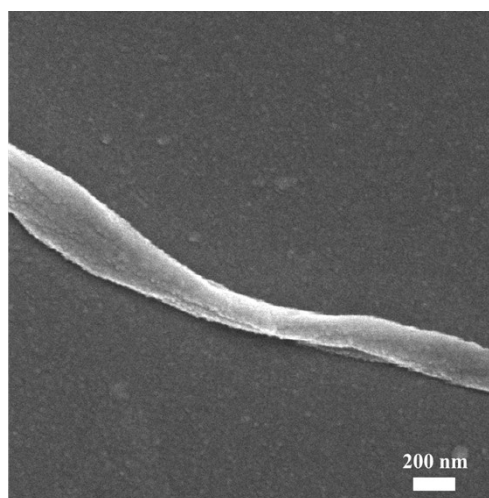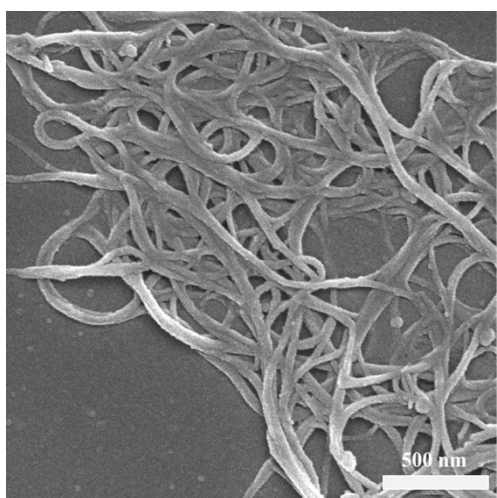


**Fig. S12** SEM images of CNT

# 9. High-Resolution Transmission Electron Micrographs
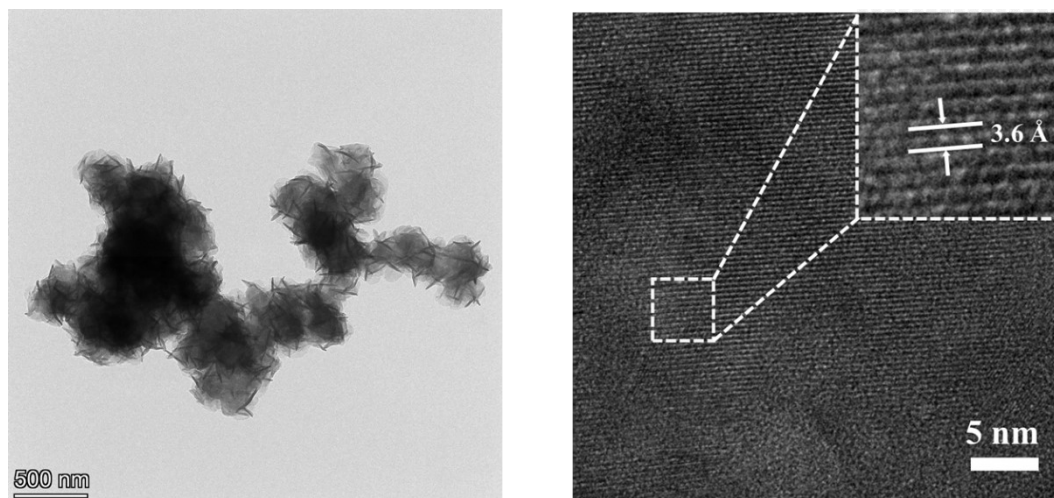


**Fig. S13** HRTEM images of COFs@BOA
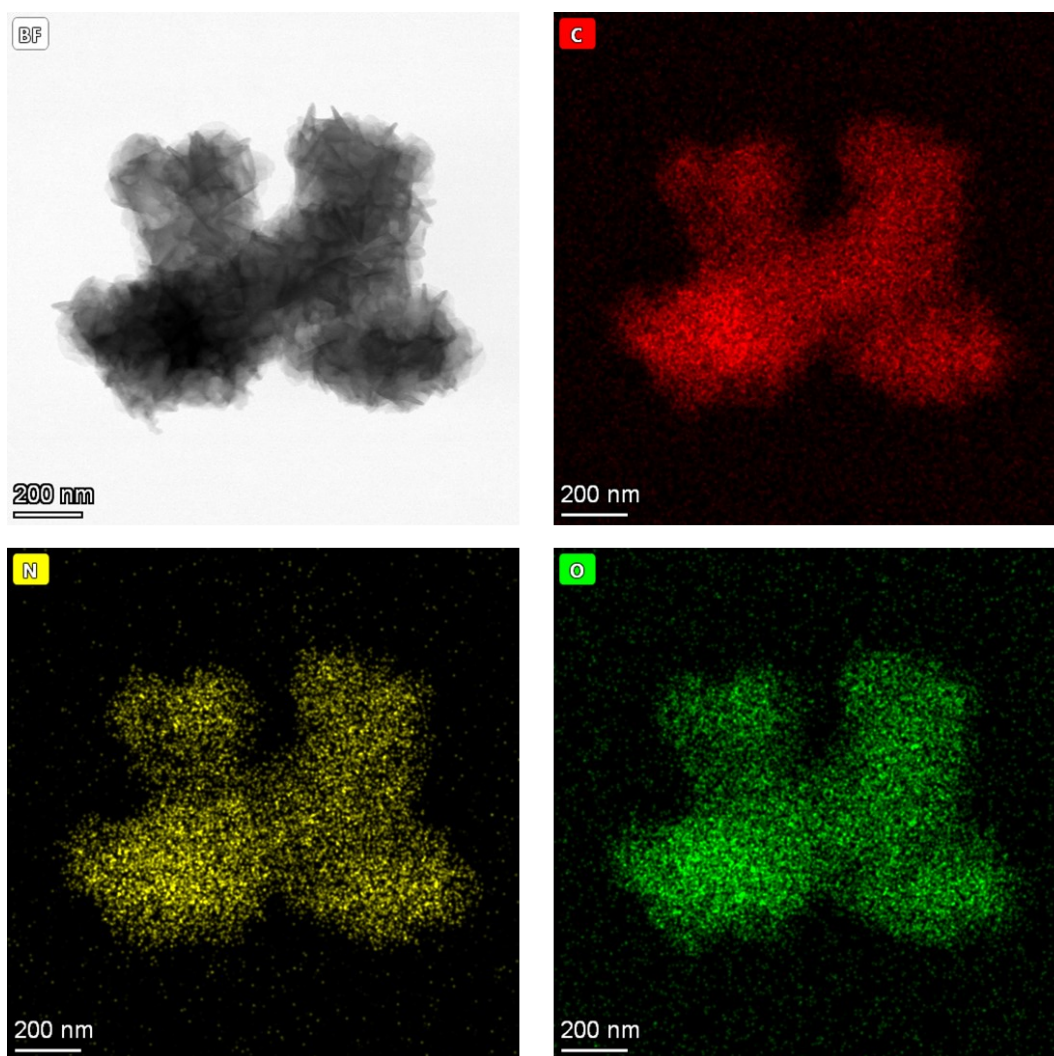
**Fig. S14** HAADF-STEM elemental mapping images of COFs@BOA
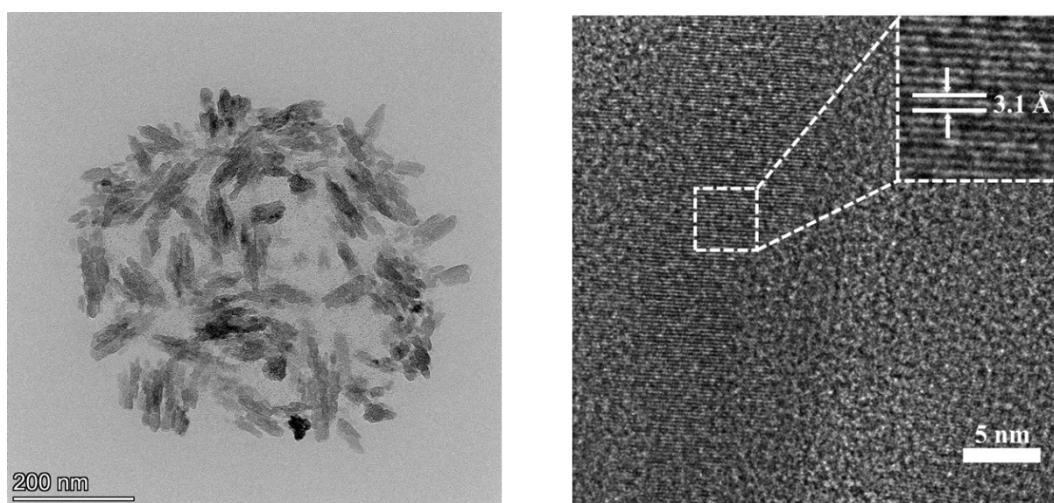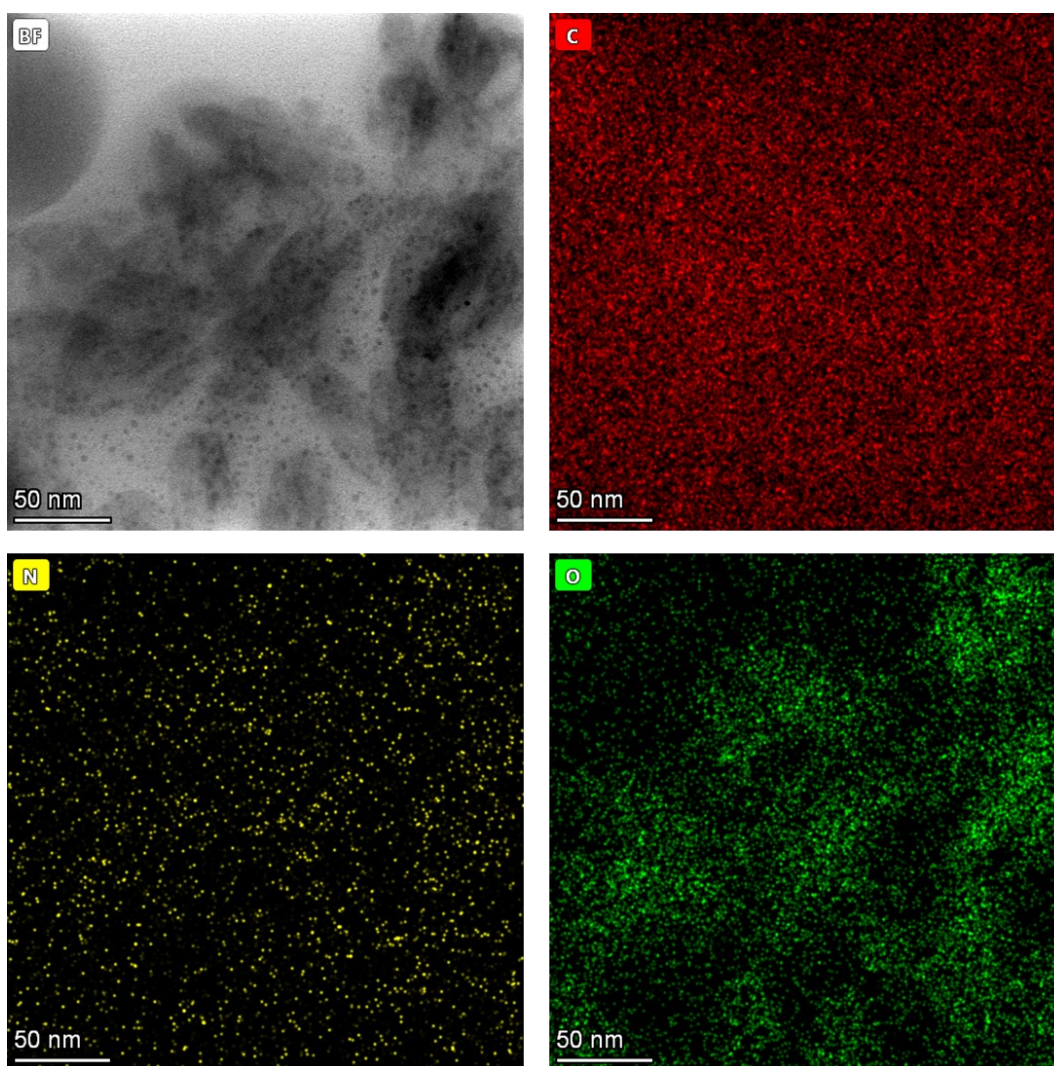


**Fig. S15** HRTEM images of COFs@IM



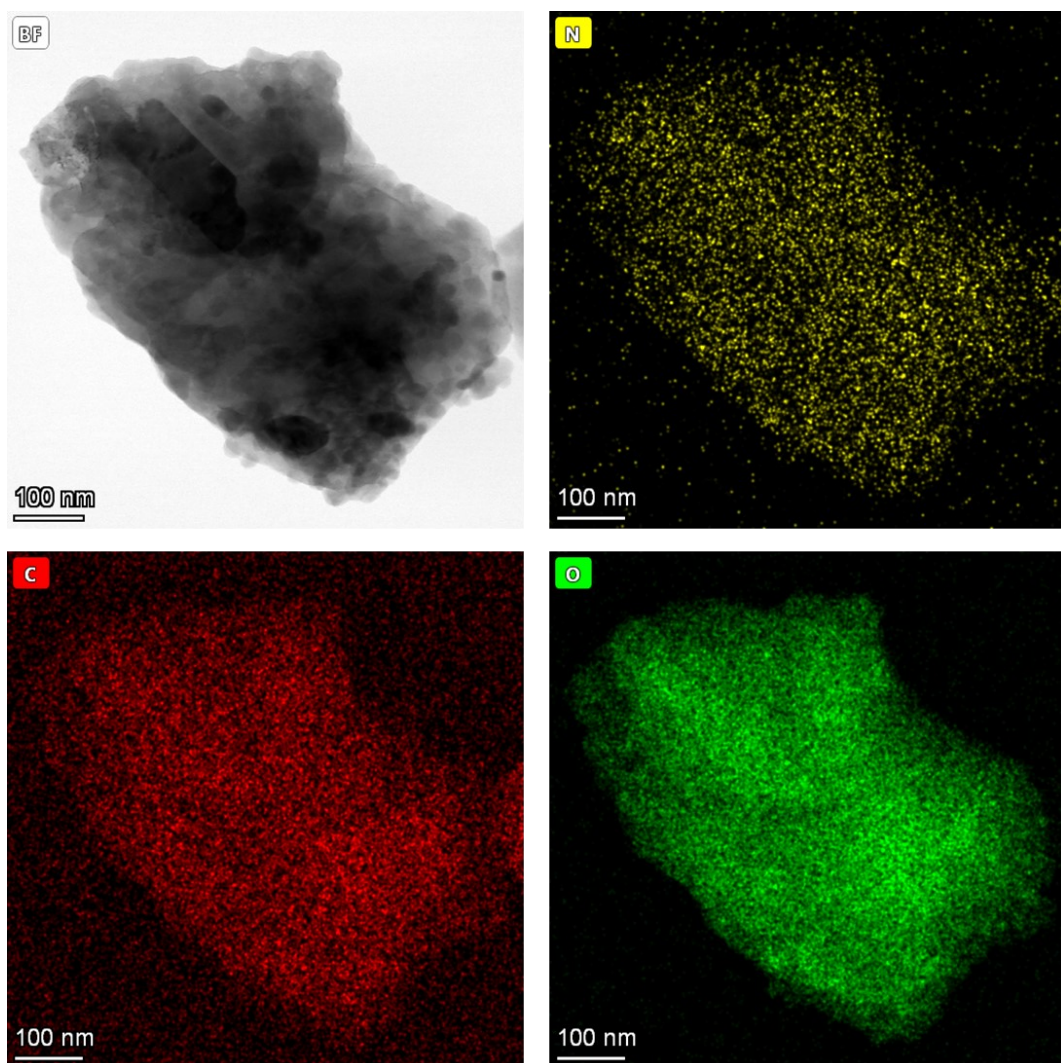**Fig. S16** HAADF-STEM elemental mapping images of COFs@IM

15

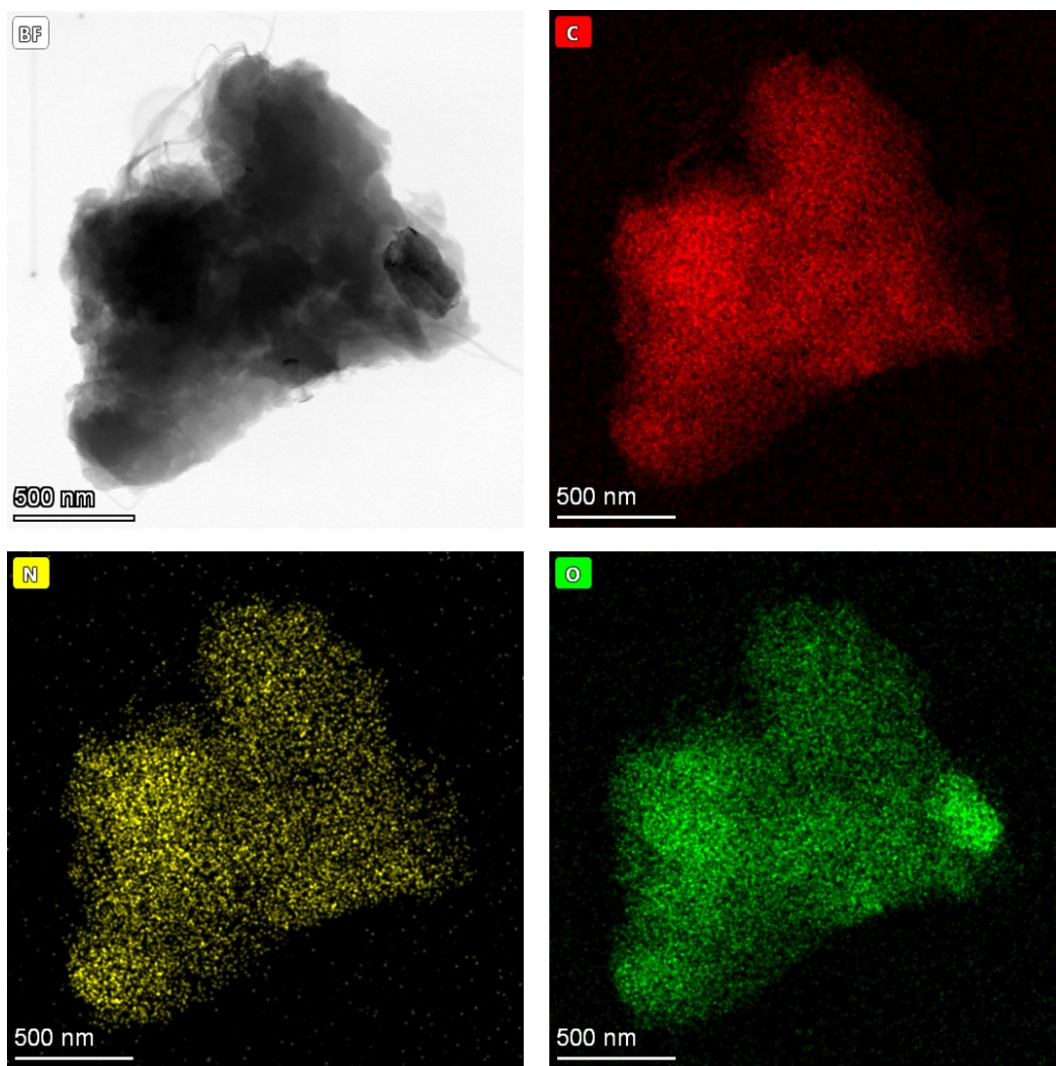**Fig. S17** HAADF-STEM elemental mapping images of COFs@BOA-30

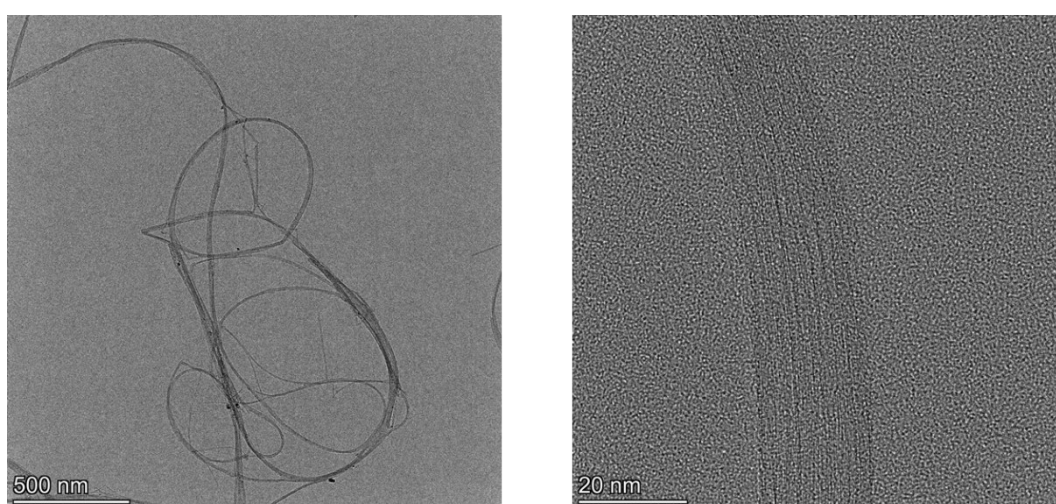**Fig. S18** HAADF-STEM elemental mapping images of COFs@IM-30



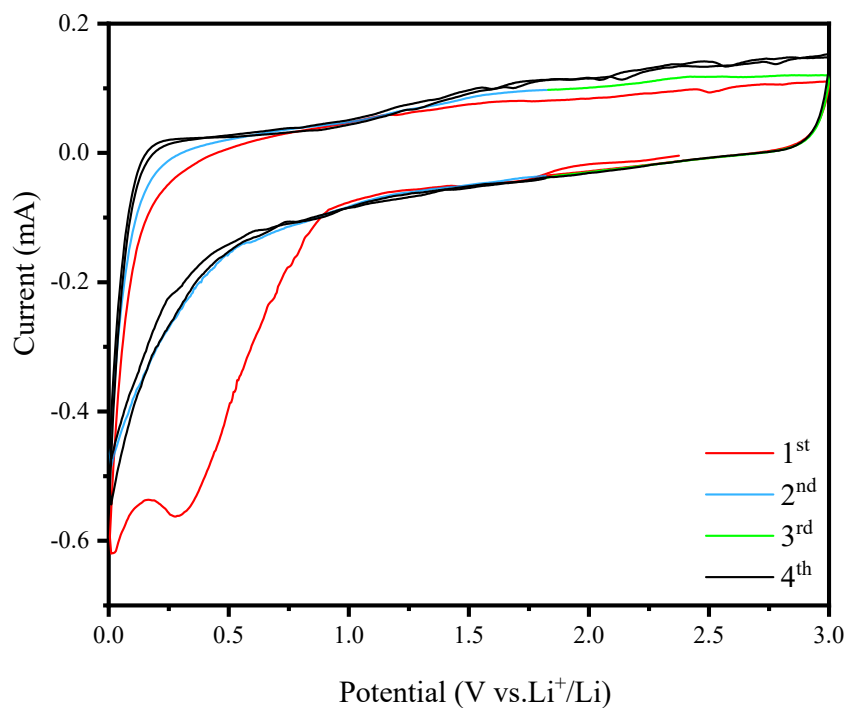**Fig. S19** HRTEM images of CNT

# 10. Electrochemical Performance



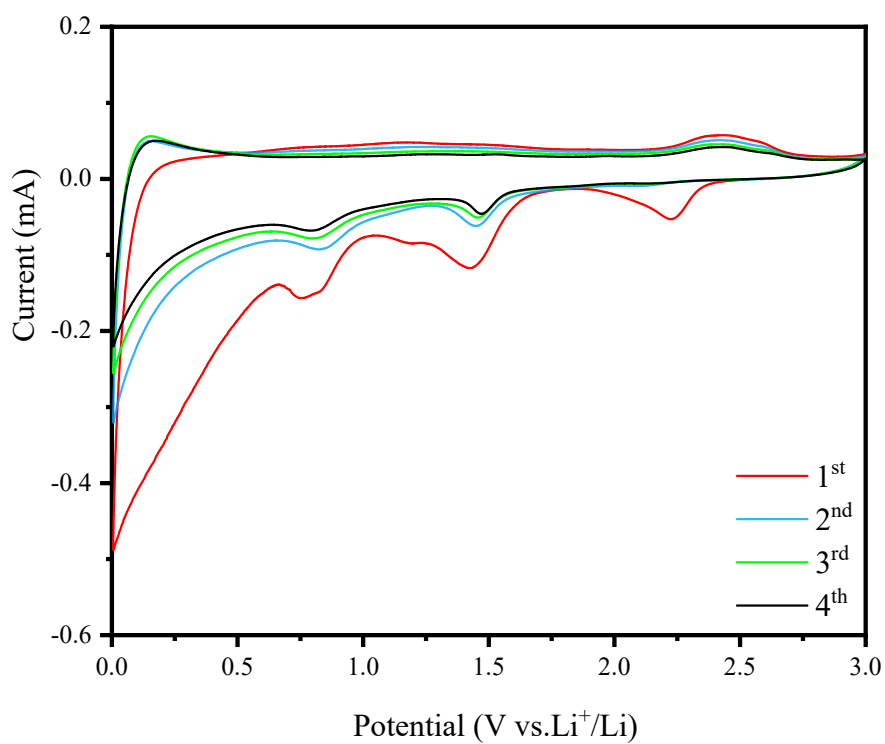**Fig. S20** The first four cycles of cyclic voltammograms of the COFs@BOA-30 based electrode

**Fig. S21** The first four cycles of cyclic voltammograms of the COFs@BOA-15 based electrode
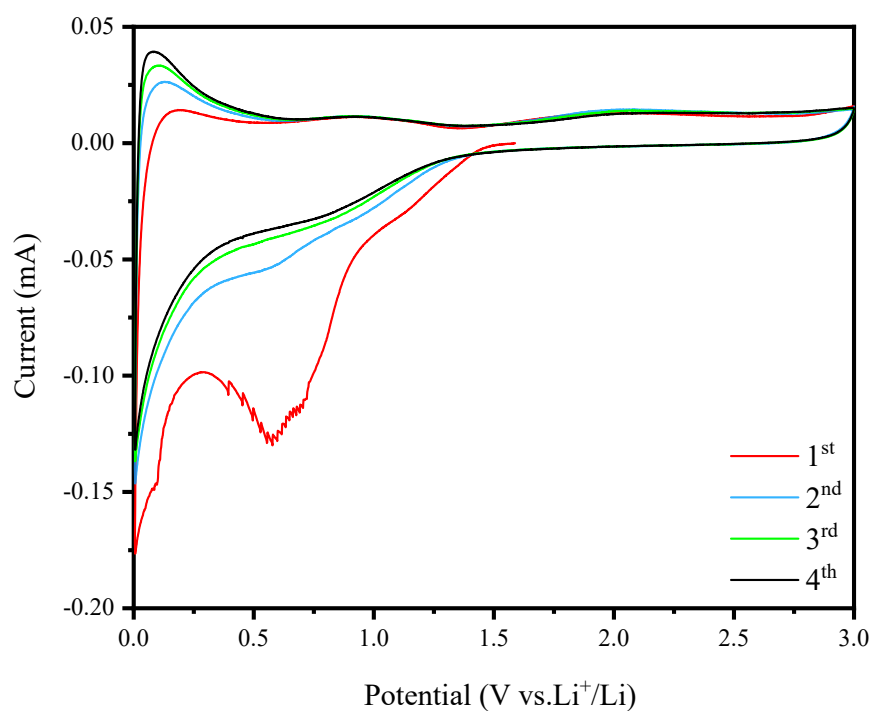


**Fig. S22** The first four cycles of cyclic voltammograms of the COFs@BOA based electrode
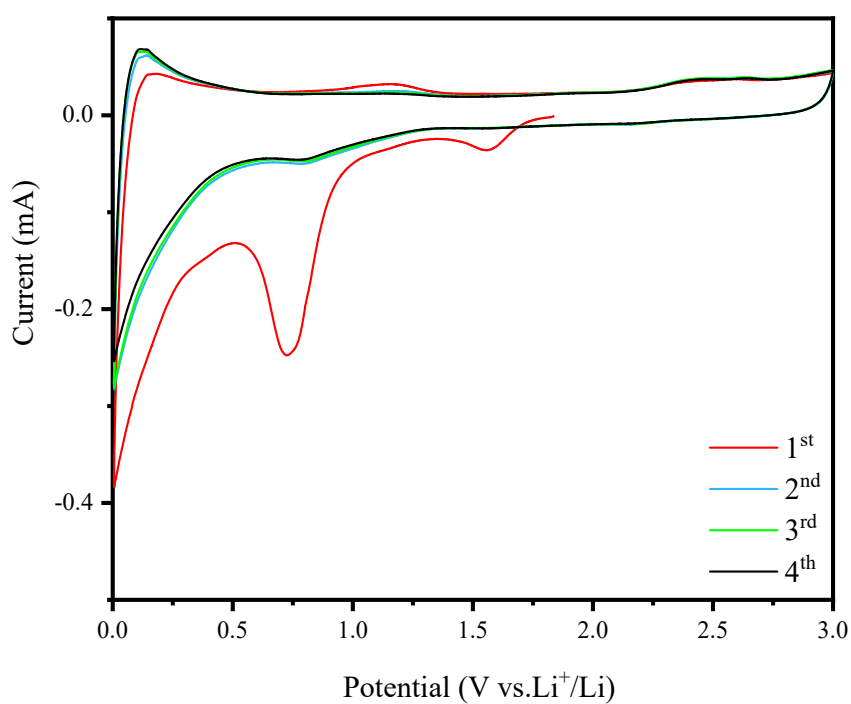
**Fig. S23** The first four cycles of cyclic voltammograms of the COFs@BOA/30 based electrode



**Fig. S24** The first four cycles of cyclic voltammograms of the COFs@IM-30 based electrode

**Fig. S25** The first four cycles of cyclic voltammograms of the COFs@IM-15 based electrode
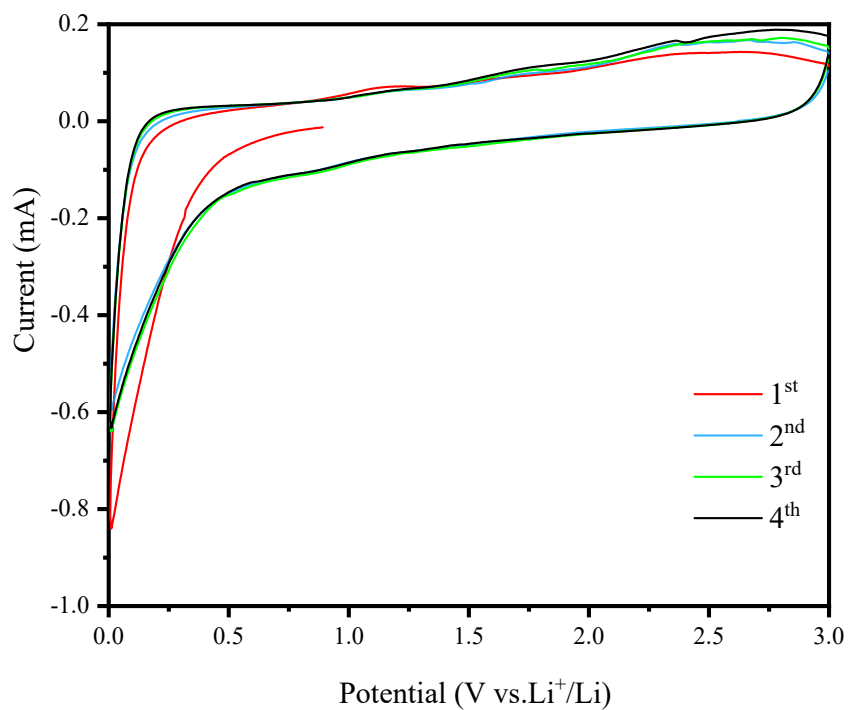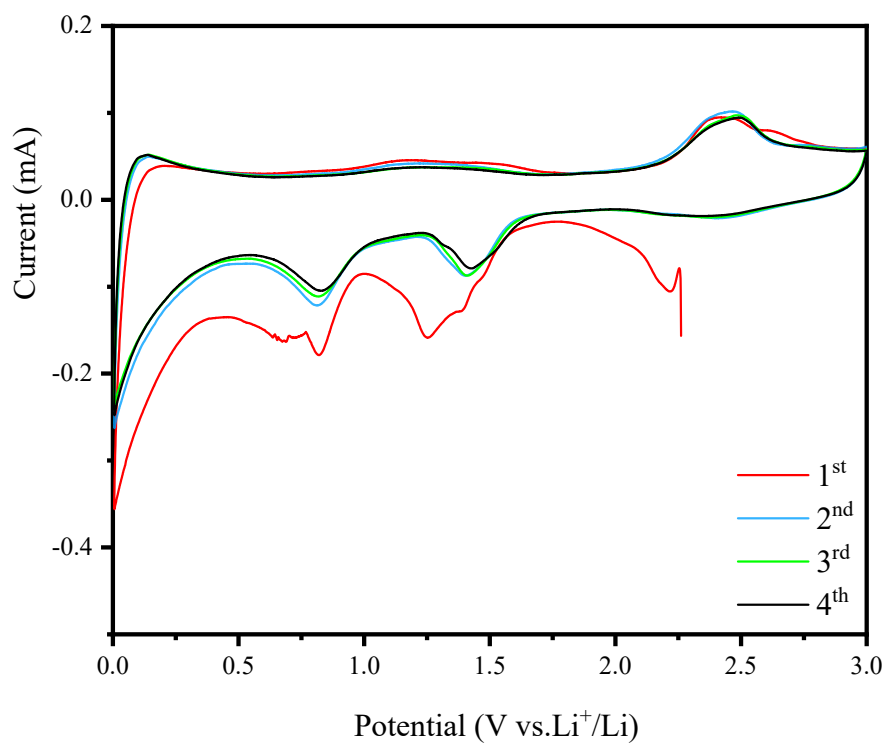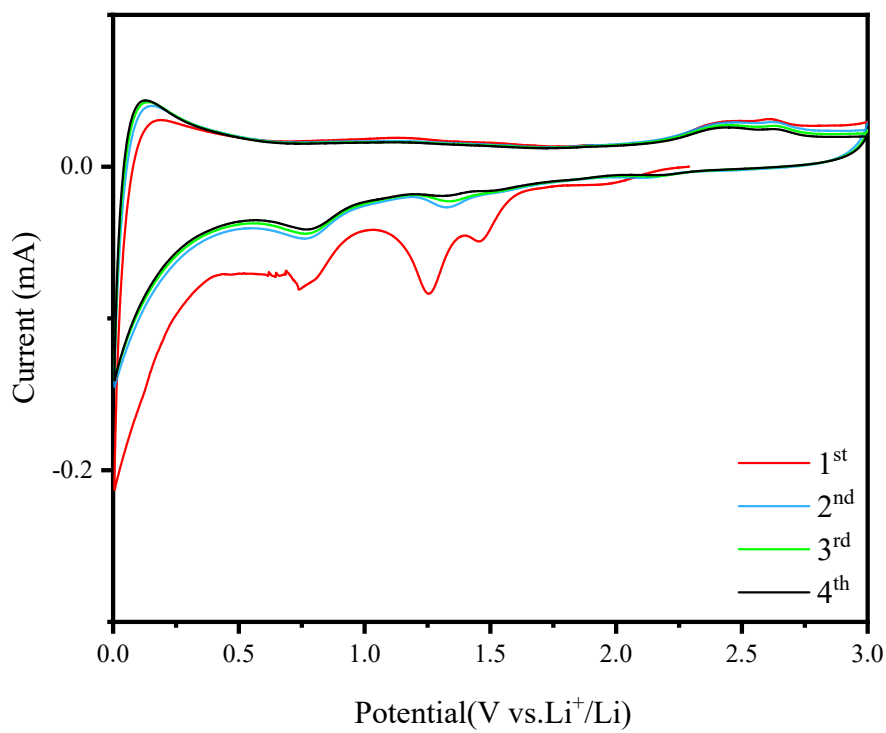
**Fig. S26** The first four cycles of cyclic voltammograms of the COFs@IM based electrode



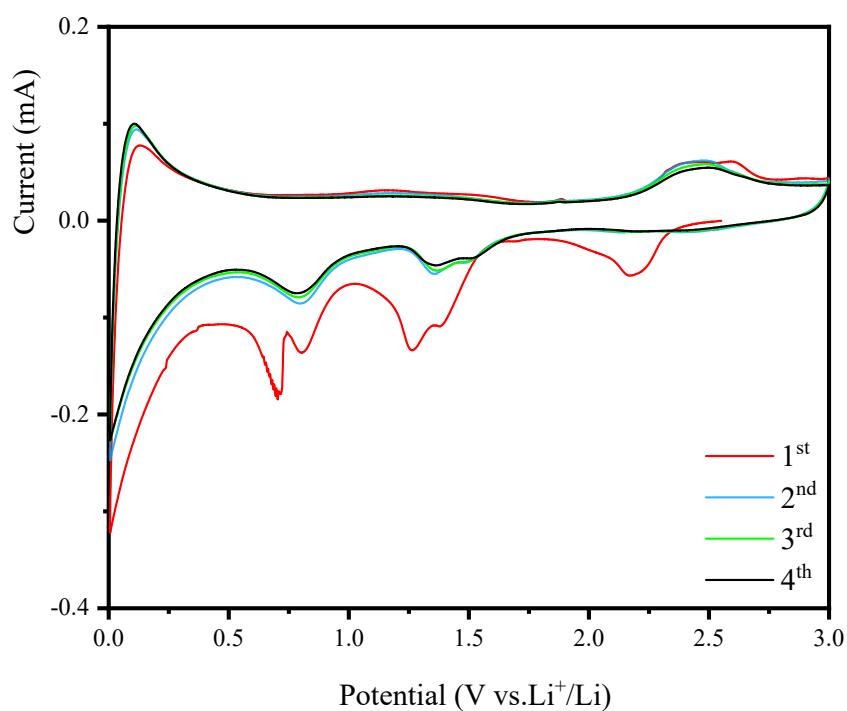**Fig. S27** The first four cycles of cyclic voltammograms of the COFs@IM/30 based electrode
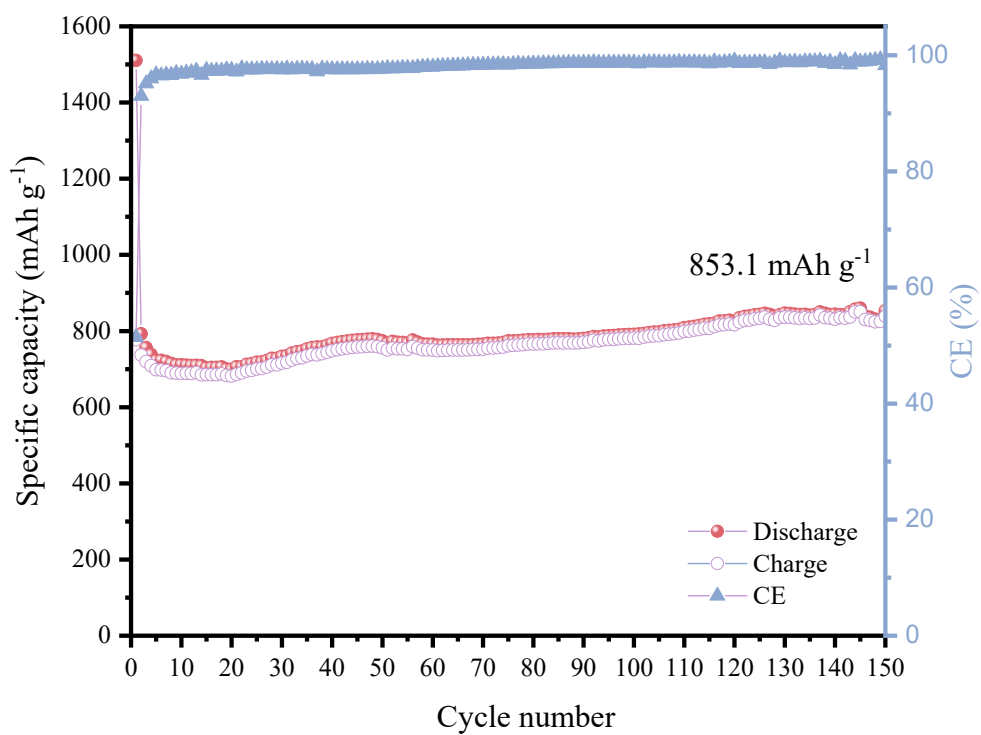
**Fig. S28** Cycling performances of the COFs@BOA-30 electrode at the current density of 100 mA g$^{-1}$.



**Fig. S29** Cycling performances of the COFs@BOA-15 electrode at the current density of 100 mA g$^{-1}$.

**Fig. S30** Cycling performances of the pure COFs@BOA electrode at the current density of 100 mA g$^{-1}$.

**Fig. S31** Cycling performances of the COFs@BOA/30 electrode at the current density of 100 mA g$^{-1}$.



474 mAh g$^{-1}$

Discharge
Charge
CE

Specific capacity1(mA g$^{-1}$)

CE (%)

Cycle number
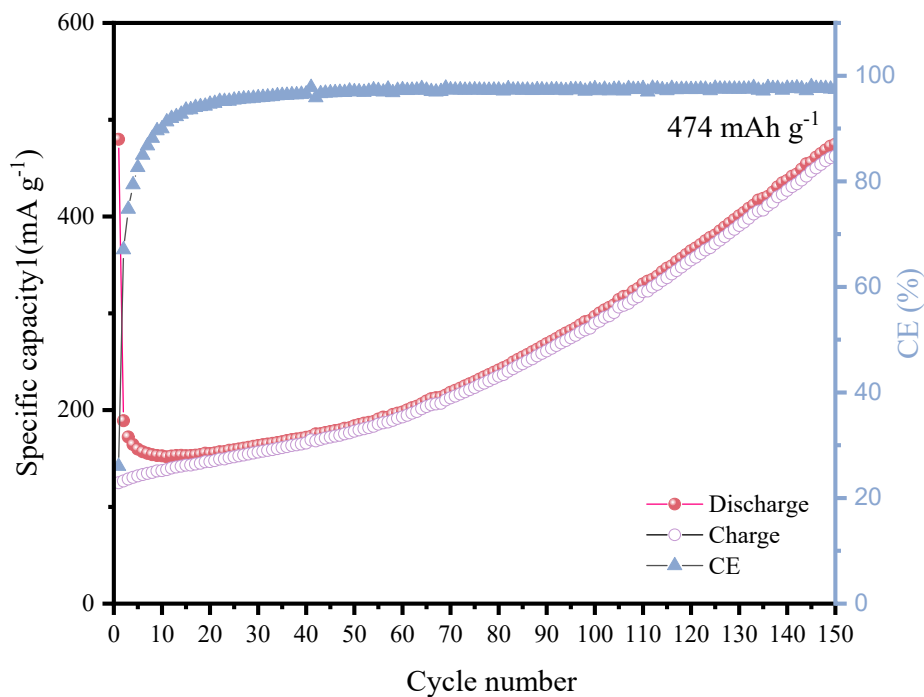
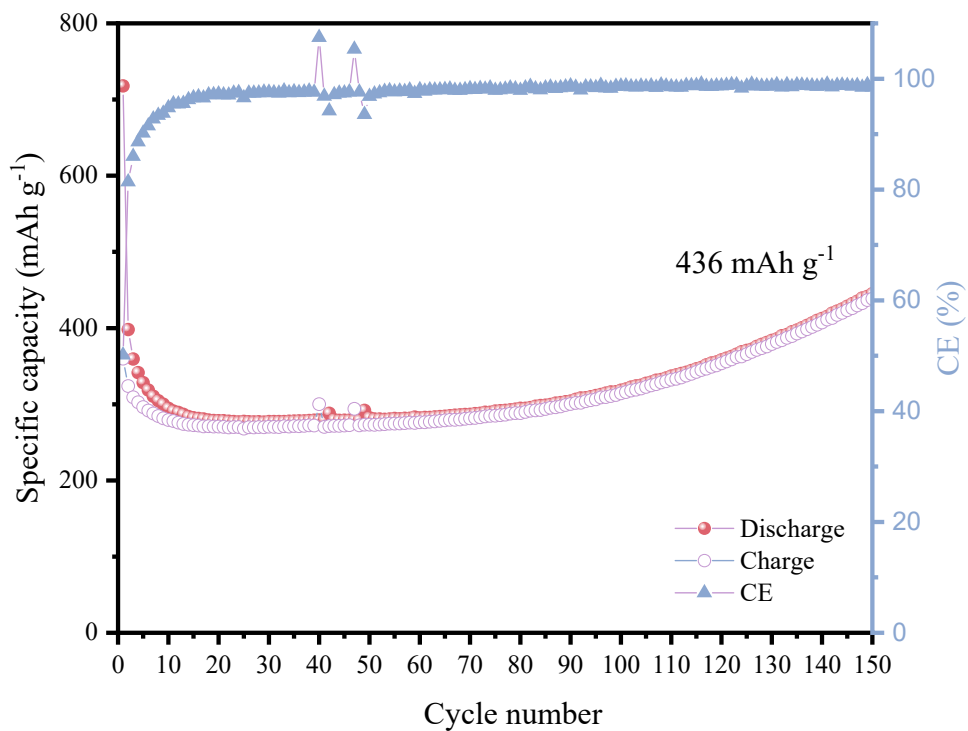**Fig. S32** Cycling performances of the COFs@IM electrode at the current density of 100 mA g$^{-1}$.
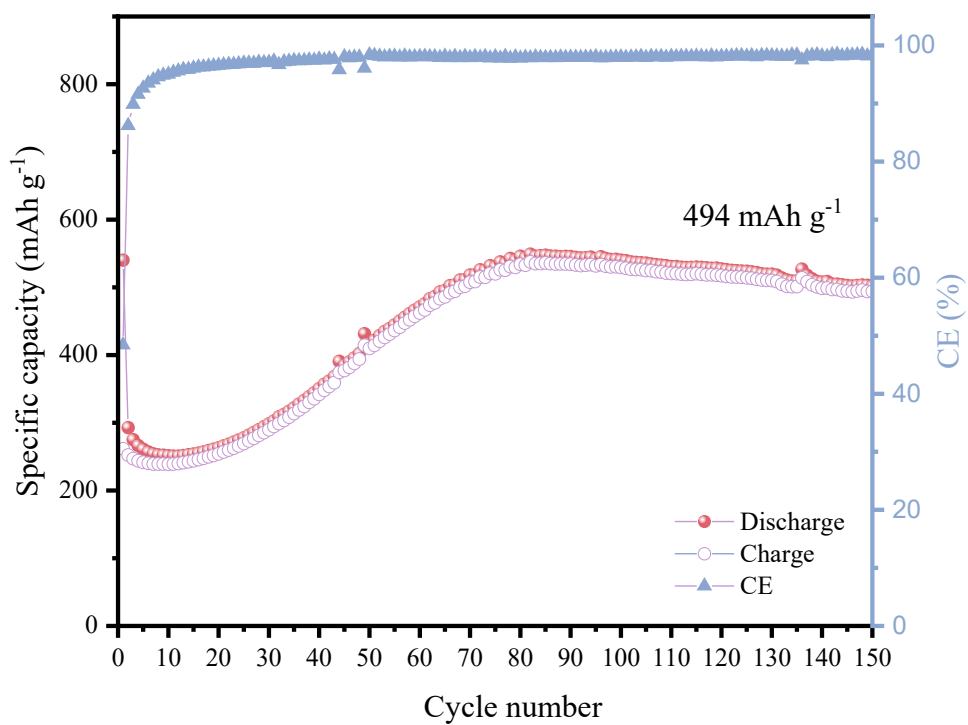
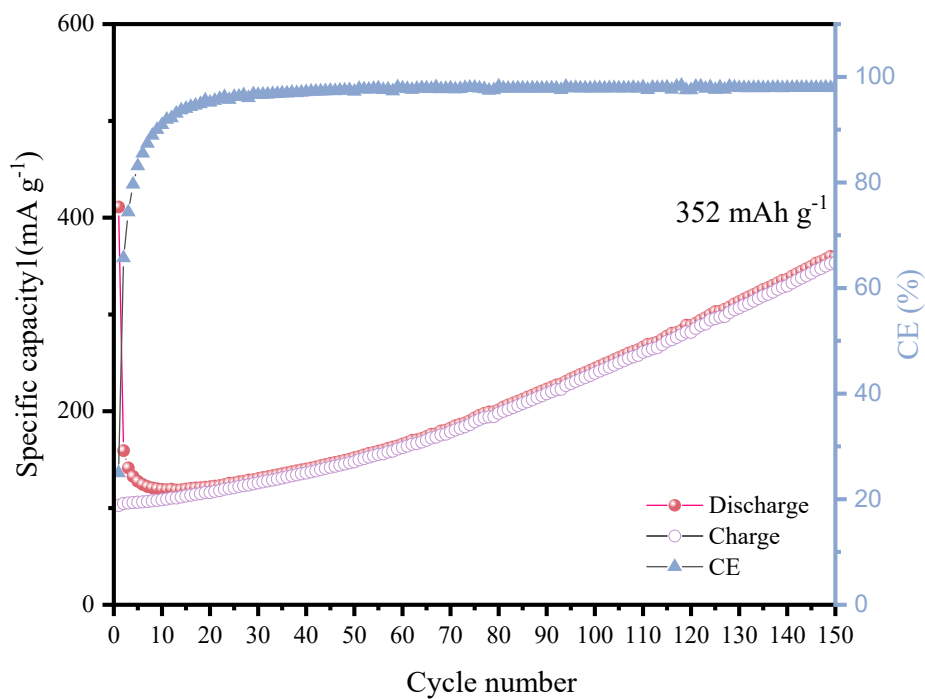**Fig. S33** Cycling performances of the COFs@IM-15 electrode at the current density of 100 mA g$^{-1}$.
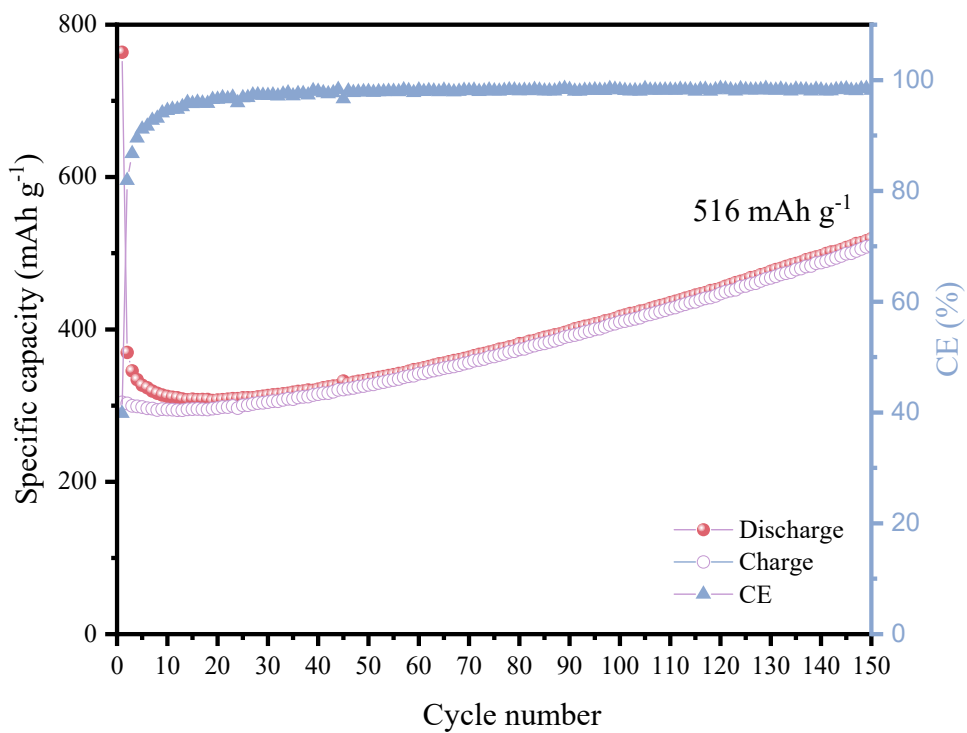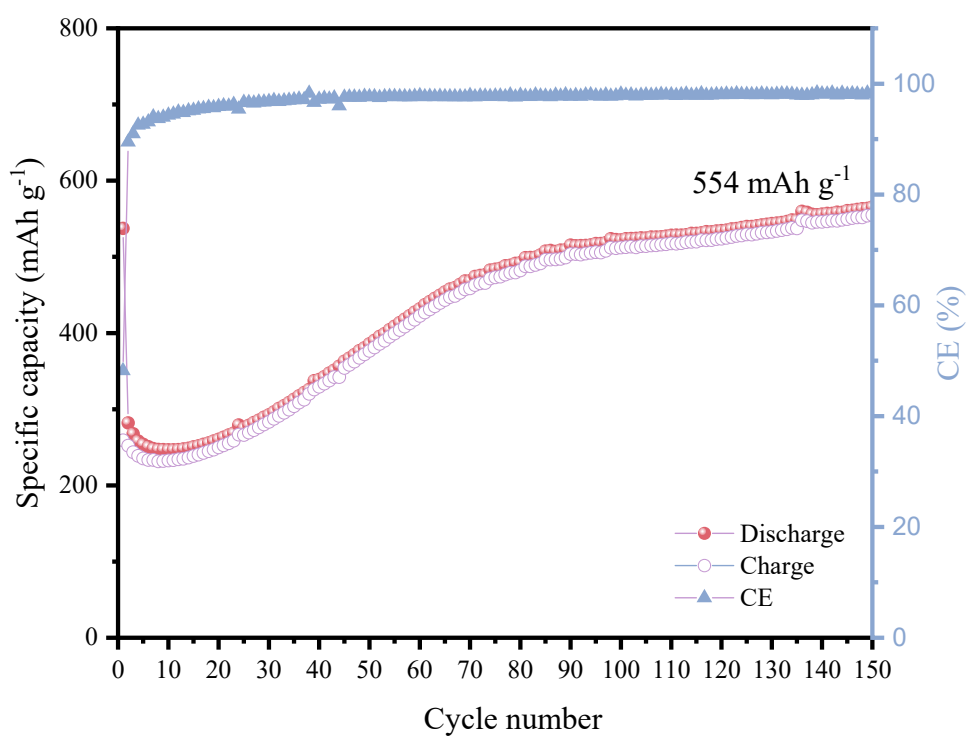
**Fig. S34** Cycling performances of the COFs@IM/30 electrode at the current density of 100 mA g$^{-1}$.



616.7 mAh g$^{-1}$
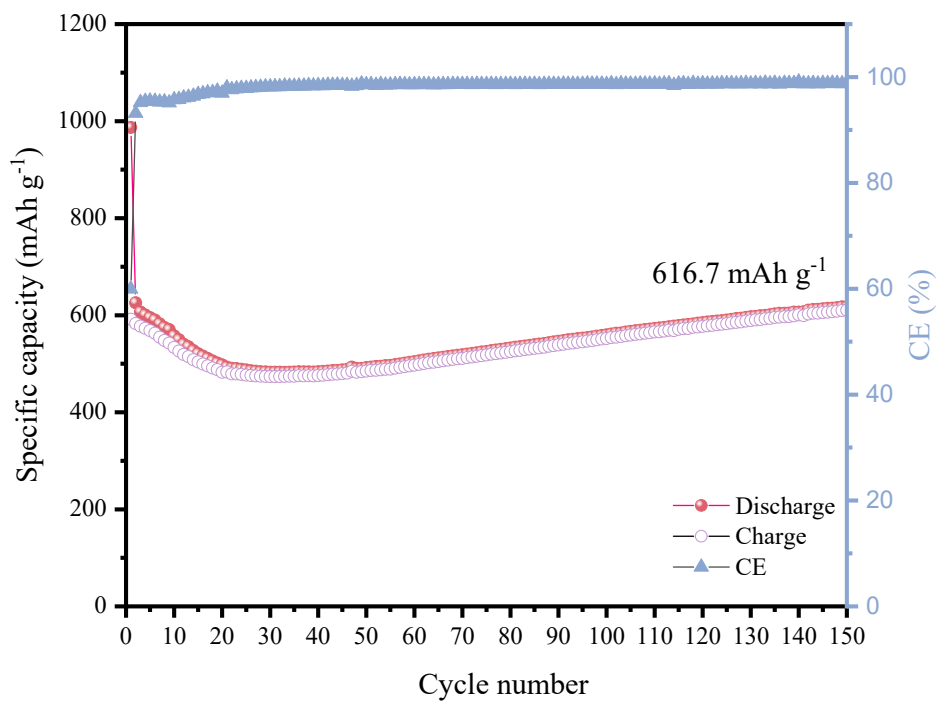
**Fig. S35** Cycling performances of the CNT electrode at the current density of 100 mA g$^{-1}$.

**Fig. S36** The rate capability of the pure COFs@IM electrode at different current densities.
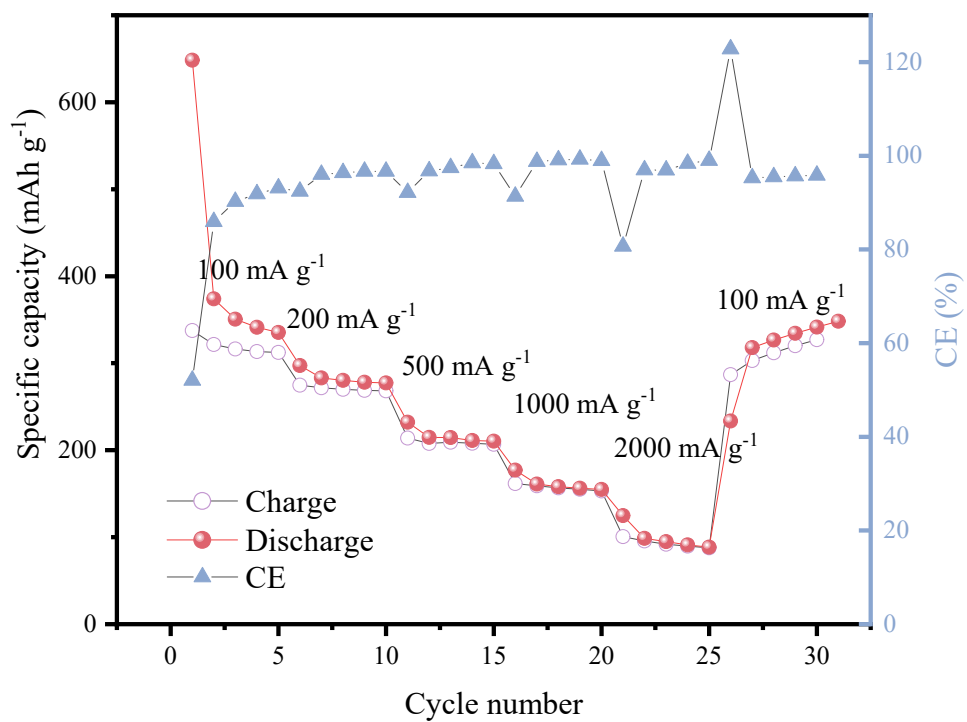


**Fig. S37** The rate capability of the COFs@IM-15 electrode at different current densities.
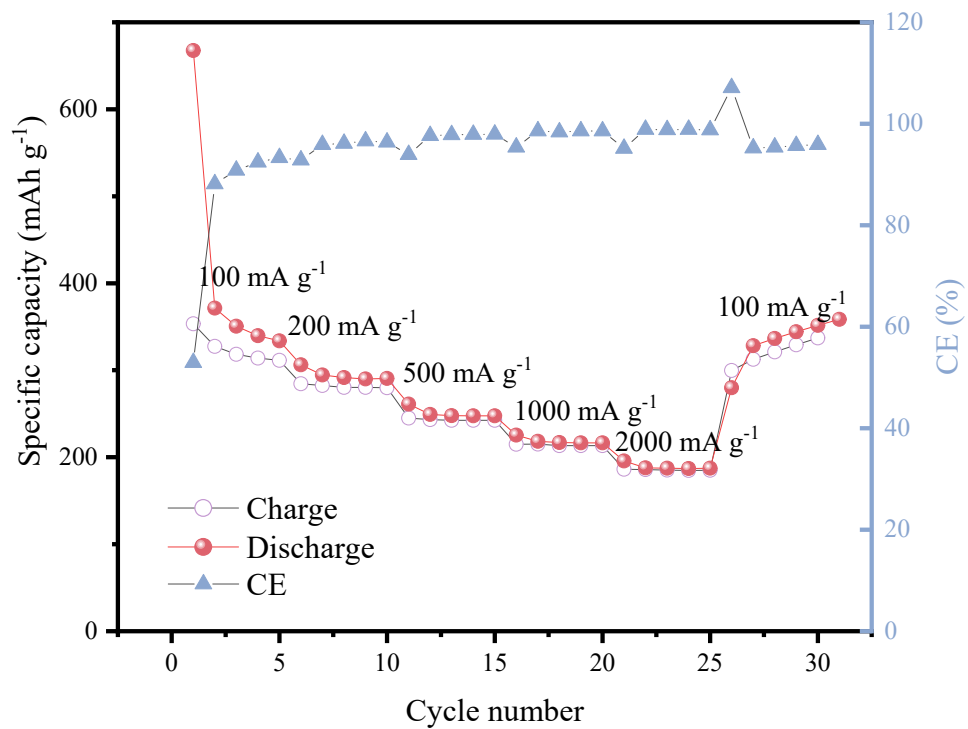
**Fig. S38** The rate capability of the COFs@IM/30 electrode at different current densities.
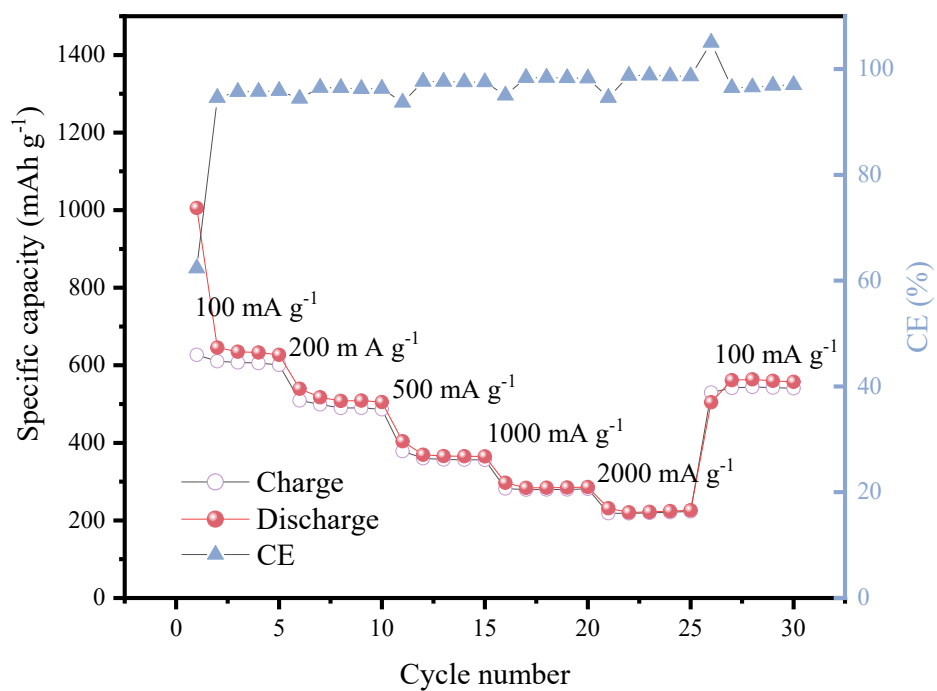
**Fig. S39** The rate capability of the pure CNT electrode at different current densities.
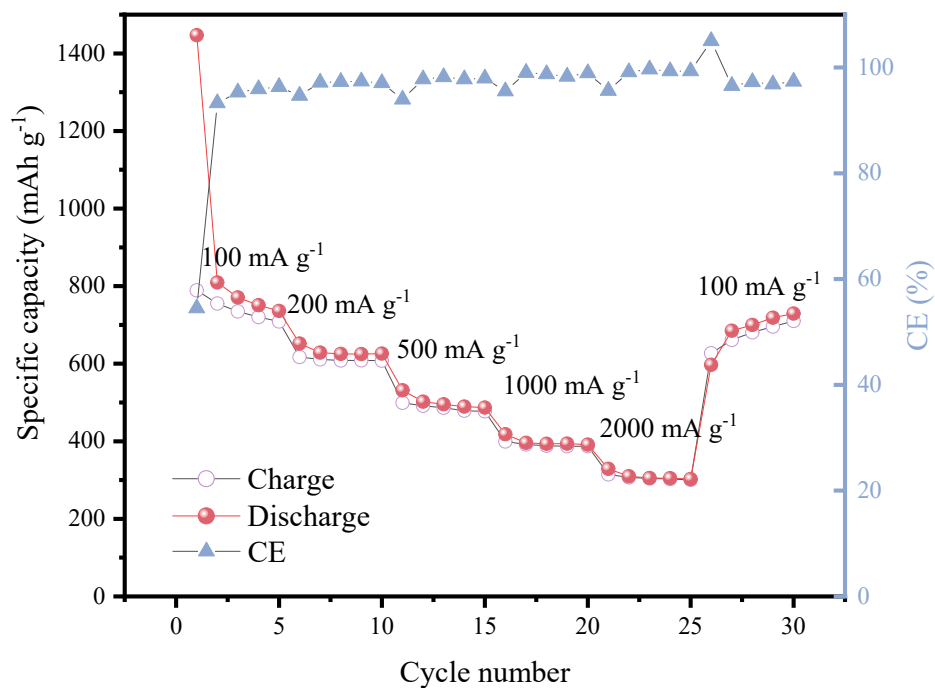


**Fig. S40** The rate capability of the COFs@BOA-30 electrode at different current densities.
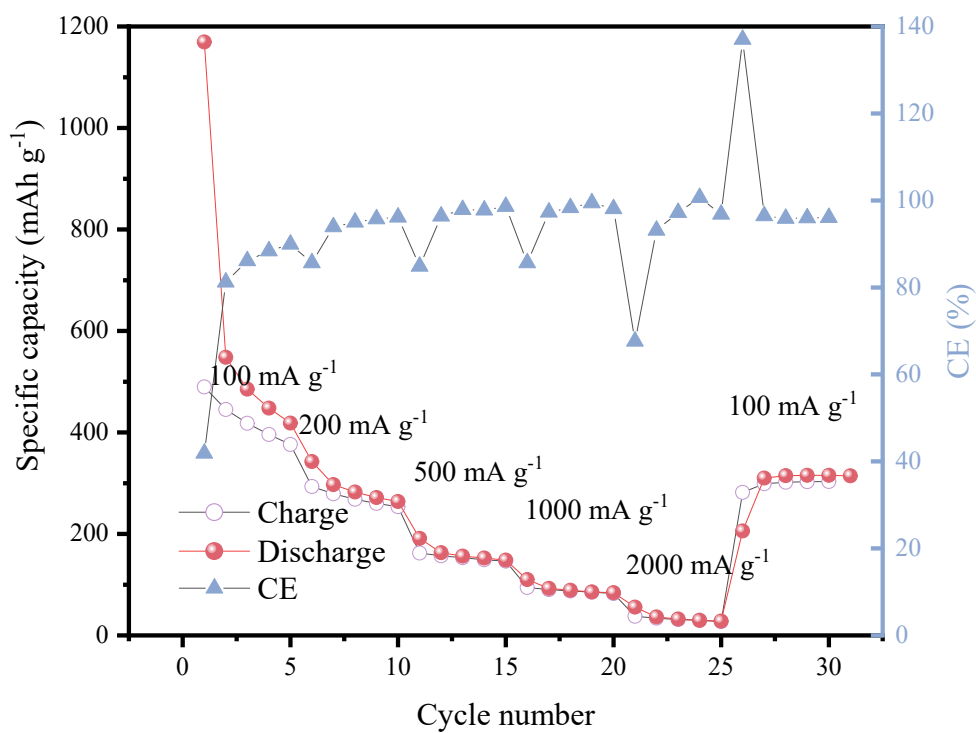
**Fig. S41** The rate capability of the COFs@BOA-15 electrode at different current densities.
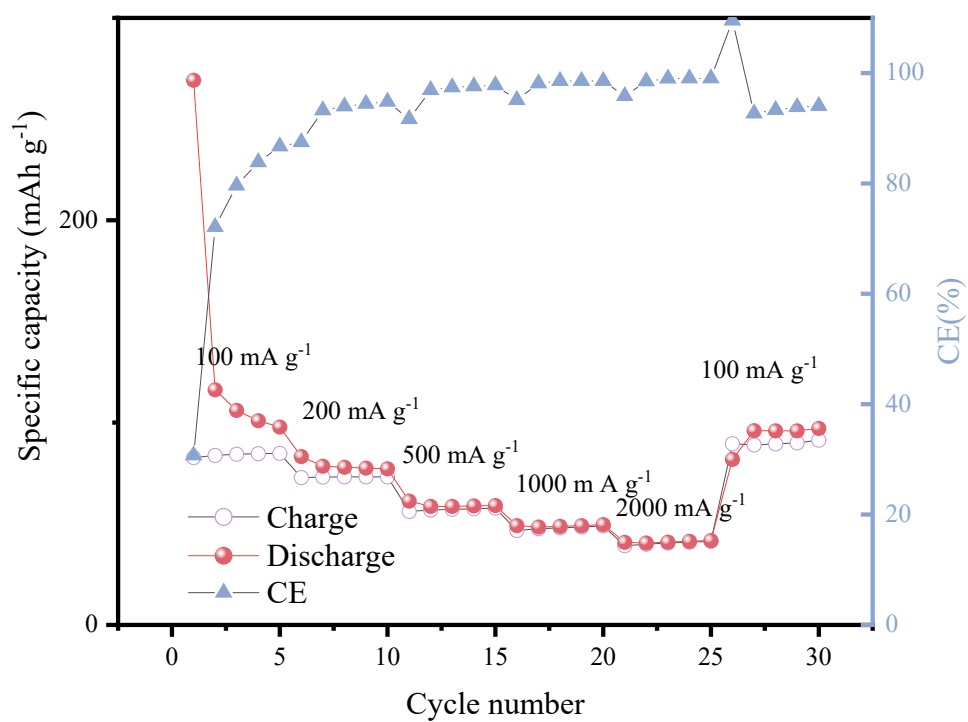


**Fig. S42** The rate capability of the pure COFs@BOA electrode at different current densities.
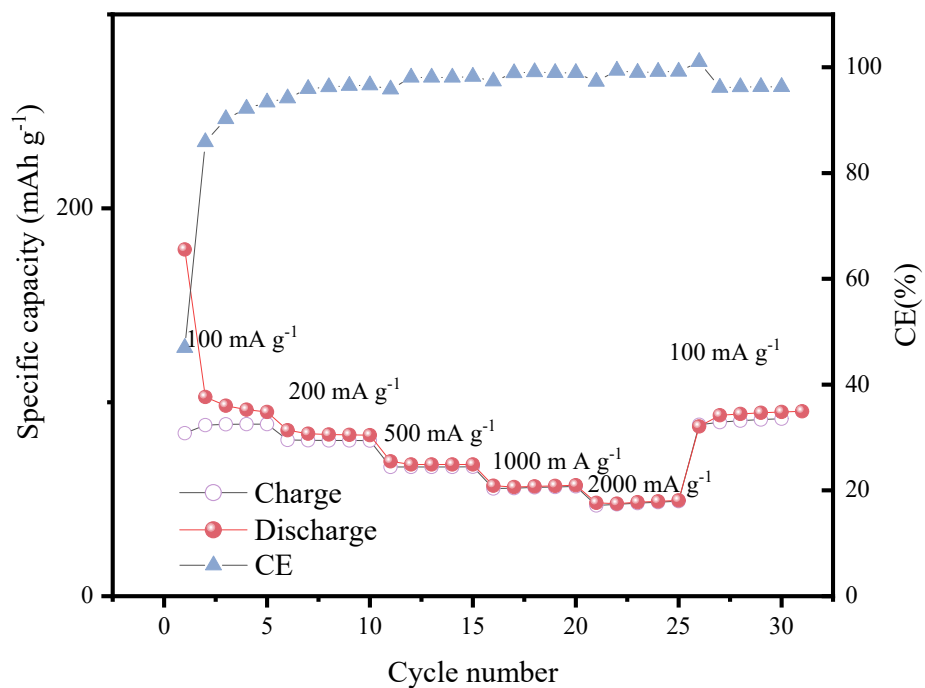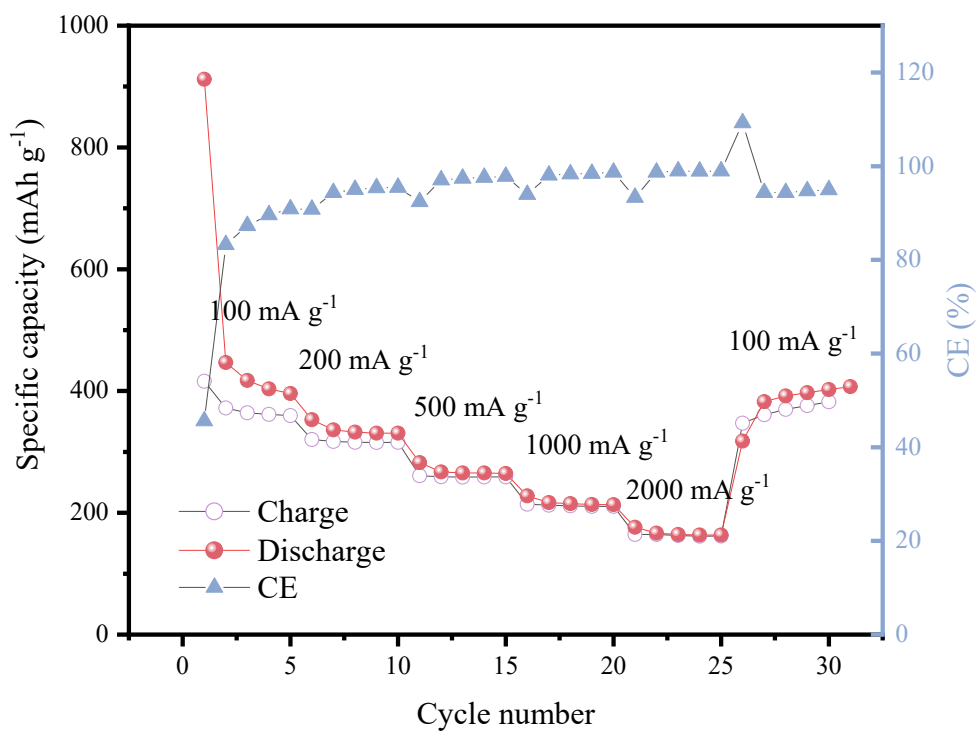
**Fig. S43** The rate capability of the COFs@BOA/30 electrode at different current densities.
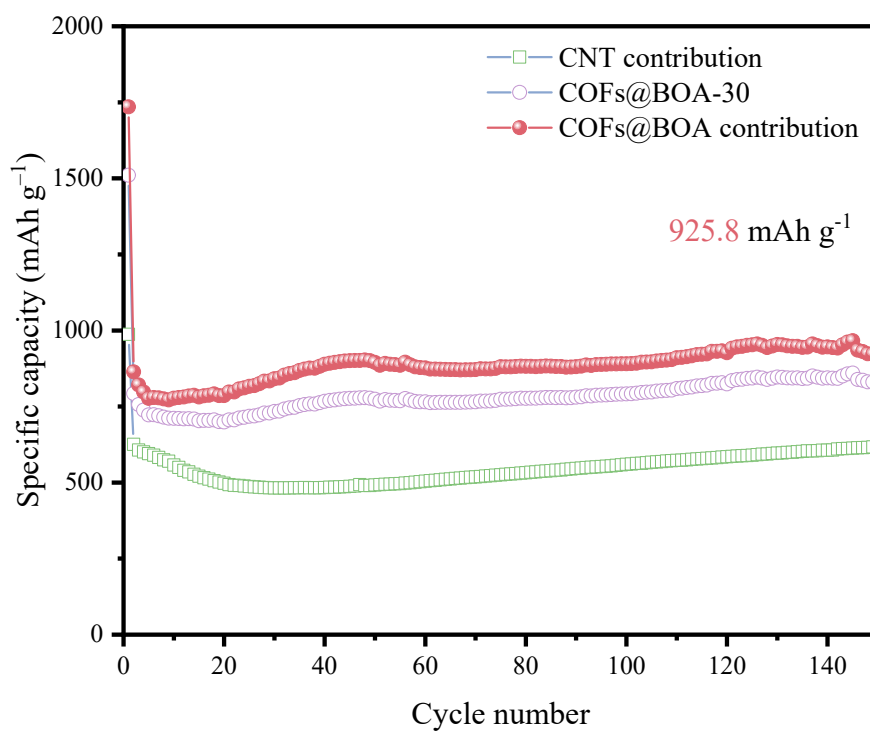


**Fig. S44** Capacity contribution of COFs@BOA (based on the mass of COFs) in COFs@BOA-30

at 100 mA $g^{-1}$.
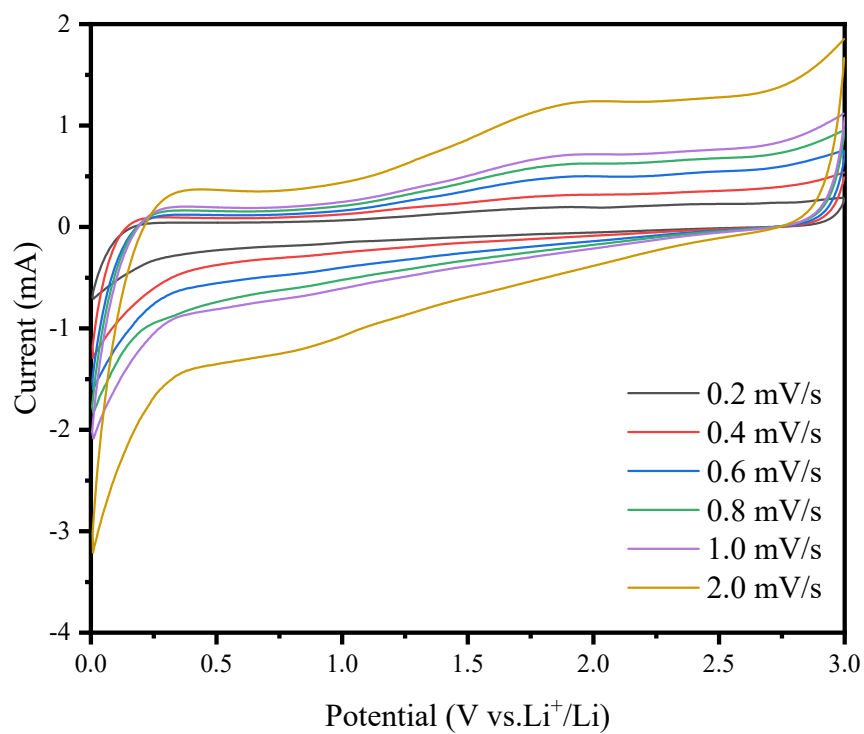


**Fig. S45** CV curves of COFs@BOA-30 anode at different scan rates (0.2, 0.4, 0.6, 0.8, 1.0 and 2.0 mV $s^{-1}$).
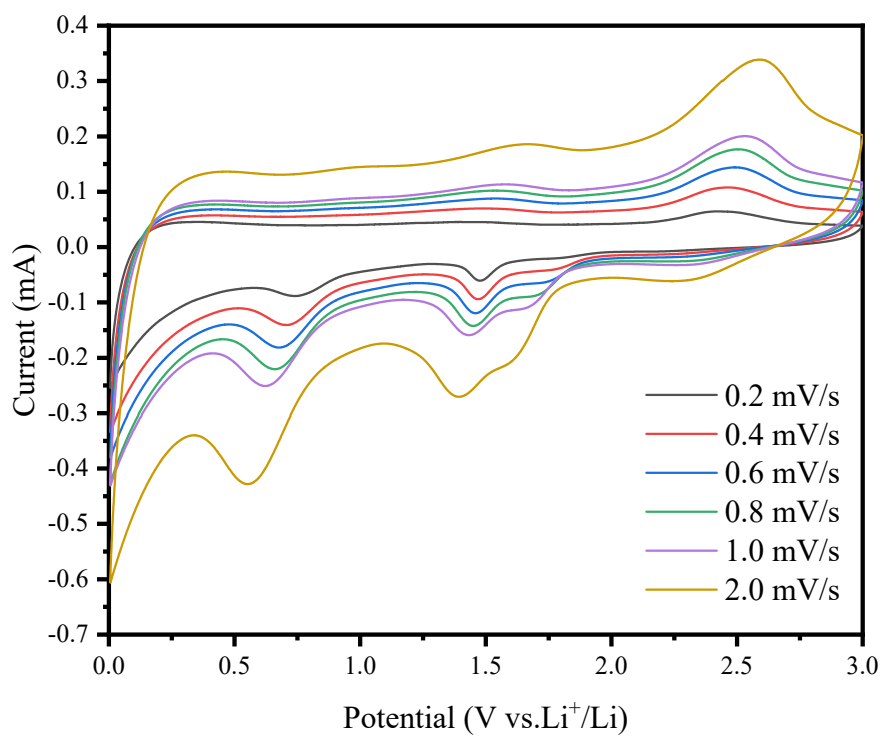
**Fig. S46** CV curves of COFs@BOA-15 anode at different scan rates (0.2, 0.4, 0.6, 0.8, 1.0 and 2.0 mV s$^{-1}$).
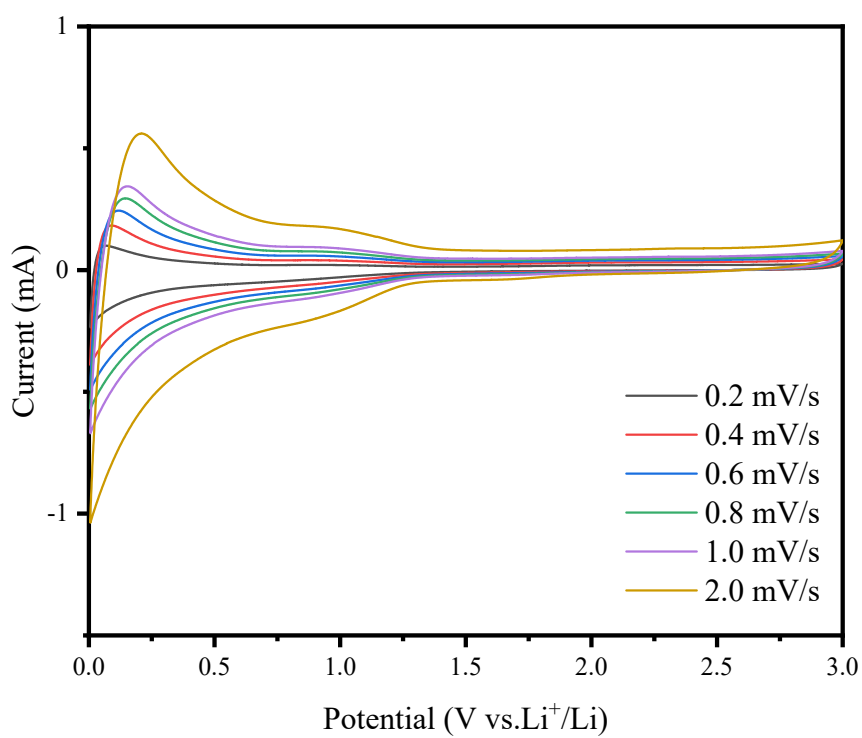
**Fig. S47** CV curves of COFs@BOA anode at different scan rates (0.2, 0.4, 0.6, 0.8, 1.0 and 2.0 mV s$^{-1}$).
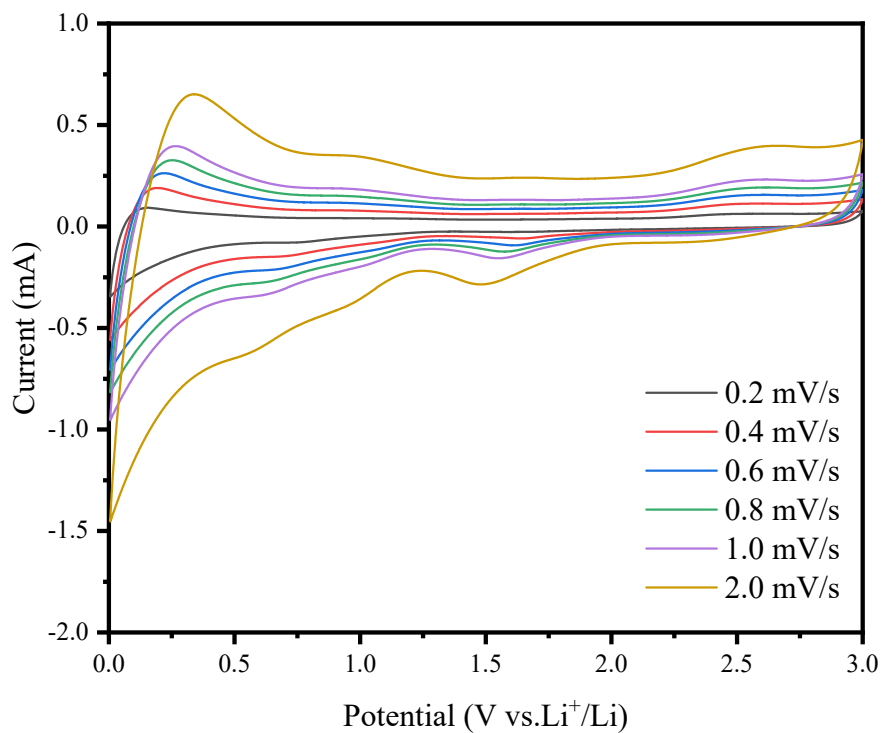


**Fig. S48** CV curves of COFs@BOA/30 anode at different scan rates (0.2, 0.4, 0.6, 0.8, 1.0 and 2.0 mV s$^{-1}$).
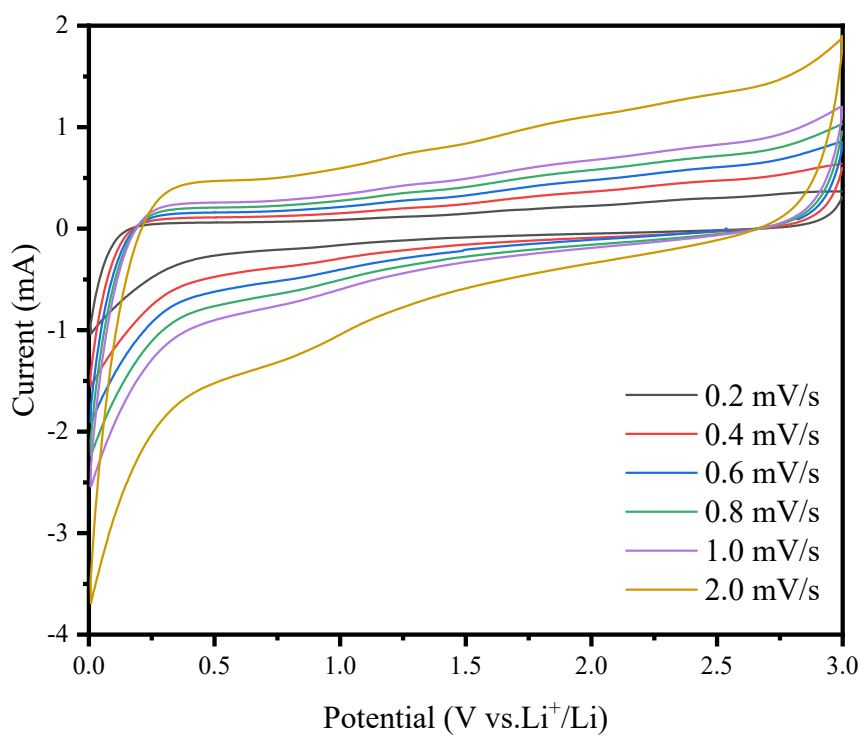
**Fig. S49** CV curves of COFs@IM-30 anode at different scan rates (0.2, 0.4, 0.6, 0.8, 1.0 and 2.0 mV s$^{-1}$).
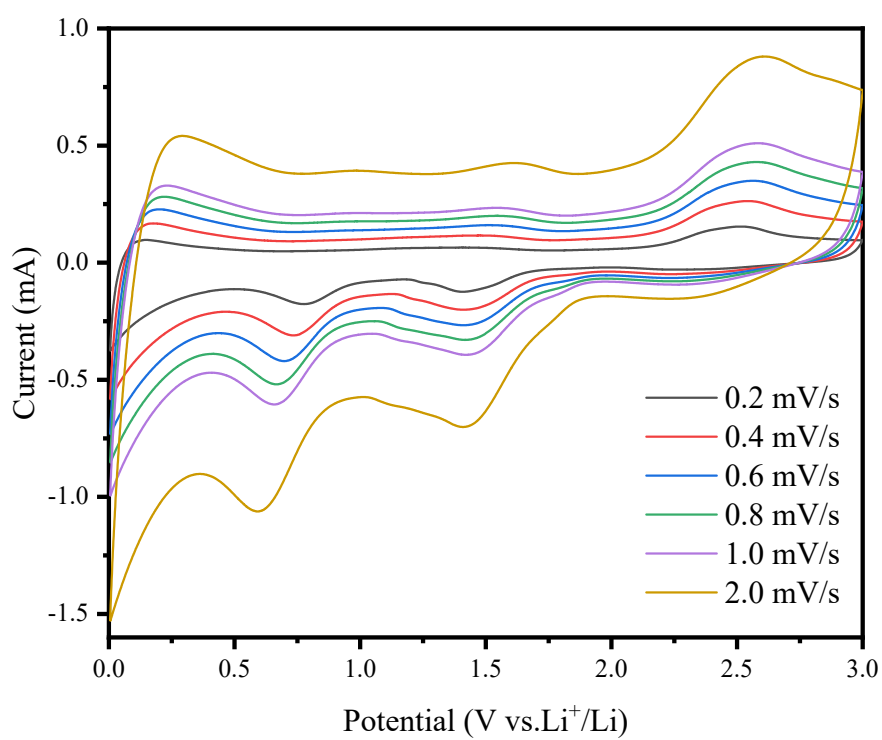
**Fig. S50** CV curves of COFs@IM-15 anode at different scan rates (0.2, 0.4, 0.6, 0.8, 1.0 and 2.0 mV s$^{-1}$).
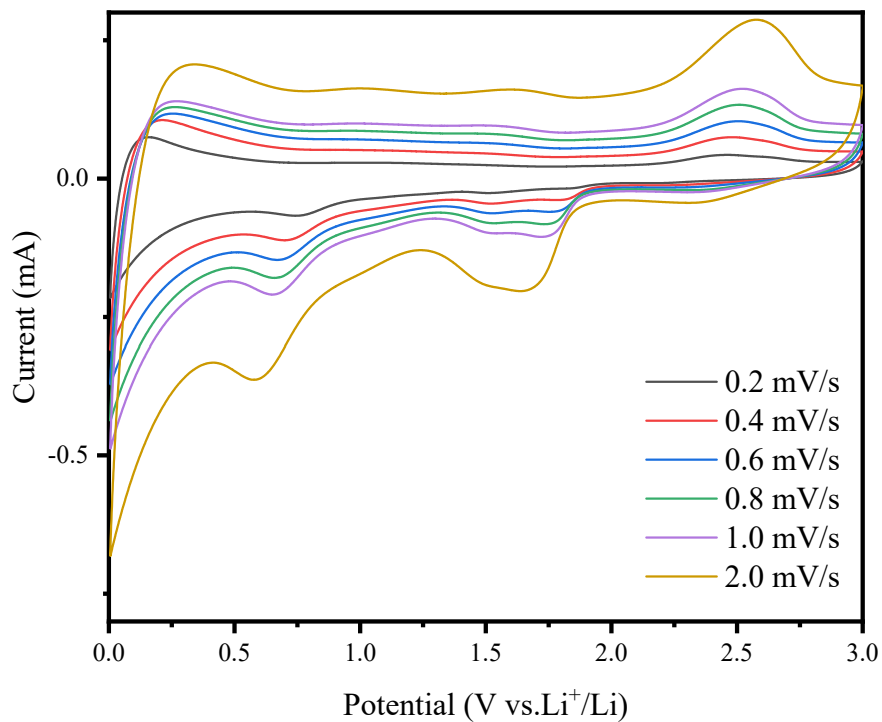


**Fig. S51** CV curves of pure COFs@IM anode at different scan rates (0.2, 0.4, 0.6, 0.8, 1.0 and 2.0 mV s$^{-1}$).
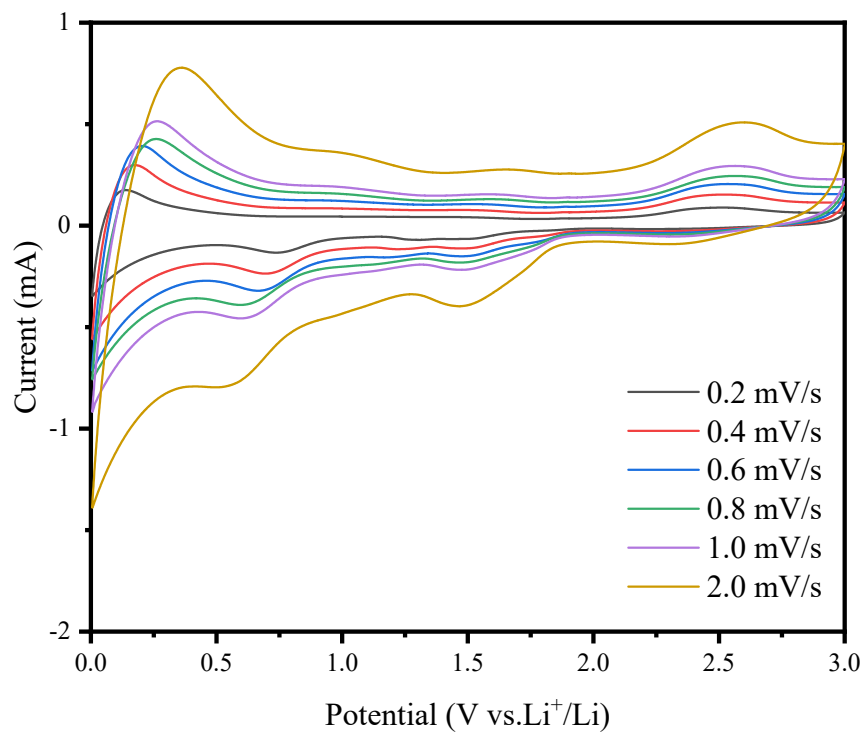
**Fig. S52** CV curves of COFs@IM/30 anode at different scan rates (0.2, 0.4, 0.6, 0.8, 1.0 and 2.0 mV s⁻¹).
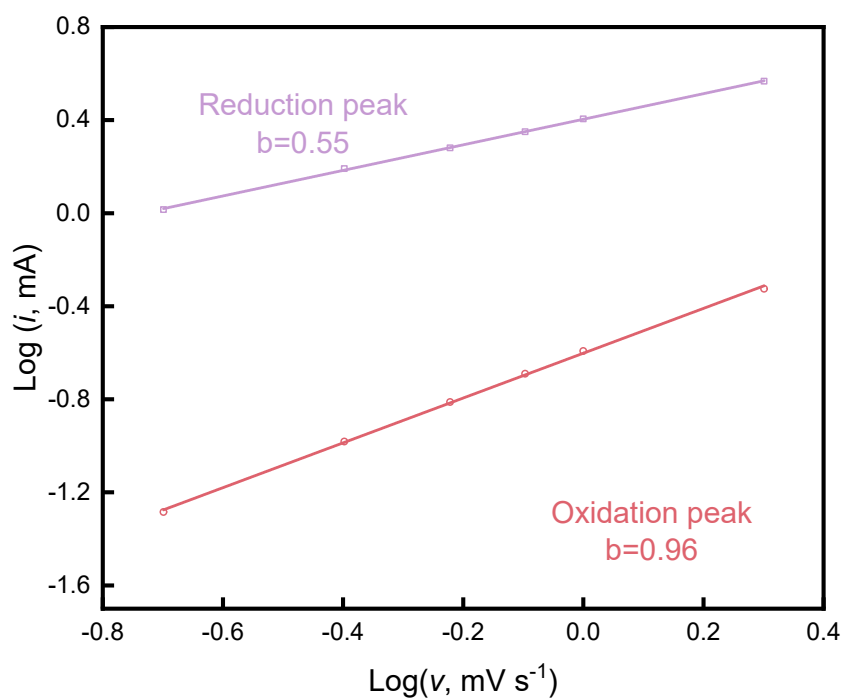
**Fig. S53** The *b*-value of COFs@IM-30 representative reduction/oxidation peaks.
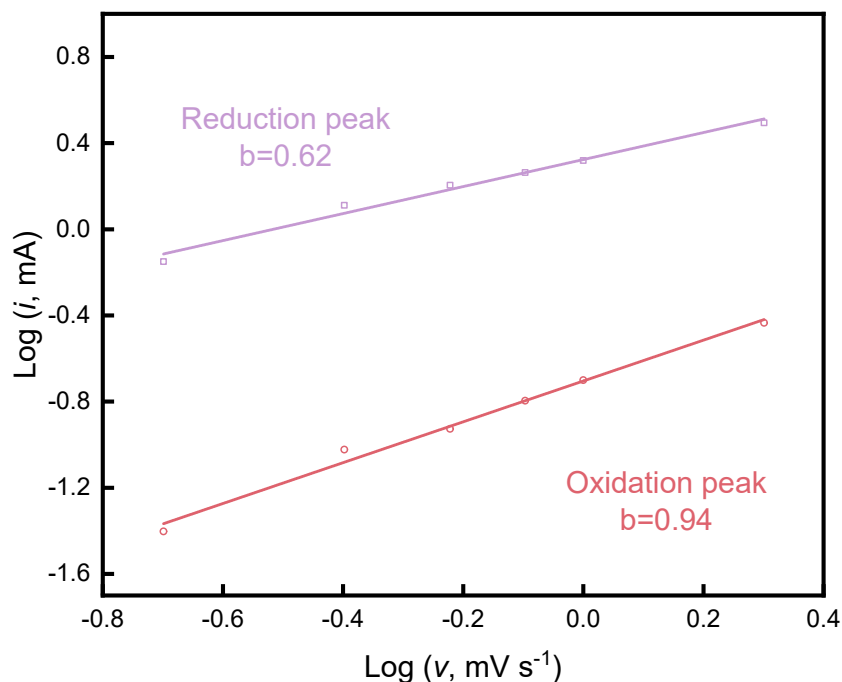


**Fig. S54** The *b*-value of COFs@BOA-30 representative reduction/oxidation peaks.
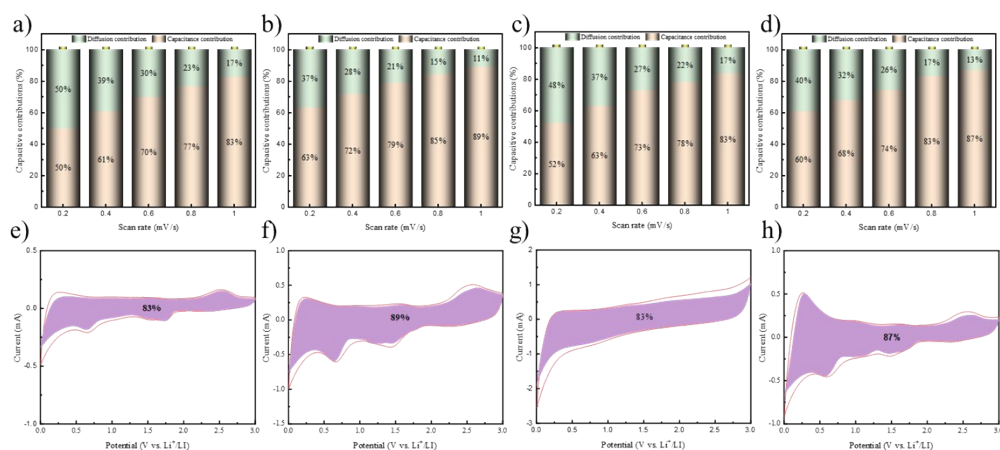


**Fig. S55** Capacitive and diffusion contribution of COFs@IM (a), COFs@IM-15 (b), COFs@IM-30 (c), and COFs@IM/30 (d) anode at multiple scan rates of 0.2-1.0 mV s$^{-1}$; Contribution of capacitance process of COFs@IM (e), COFs@IM-15 (f), COFs@IM-30 (g), and COFs@IM/30 (h) at the scan rate of 1.0 mV s$^{-1}$.
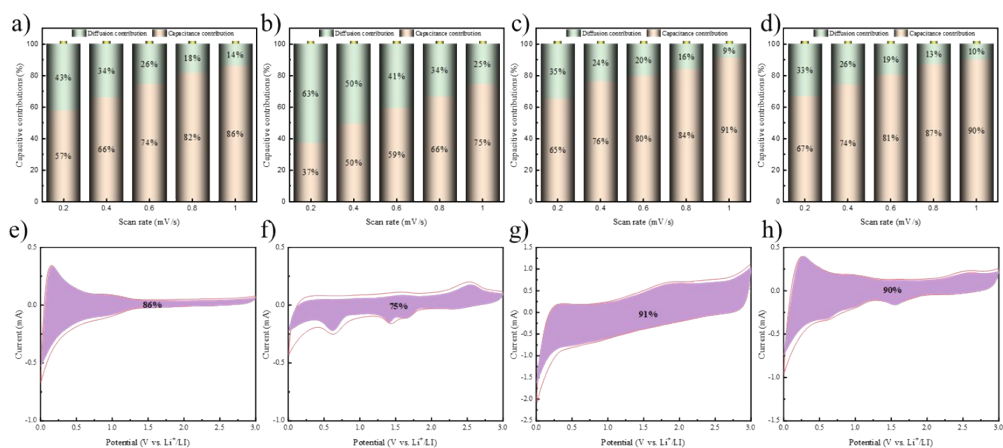
**Fig. S56** Capacitive and diffusion contribution of COFs@BOA (a), COFs@BOA-15 (b), COFs@BOA-30 (c), and COFs@BOA/30 (d) anode at multiple scan rates of 0.2-1.0 mV s$^{-1}$; Contribution of capacitance process of COFs@BOA (e), COFs@BOA-15 (f), COFs@BOA-30 (g), and COFs@BOA/30 (h) at the scan rate of 1.0 mV s$^{-1}$.
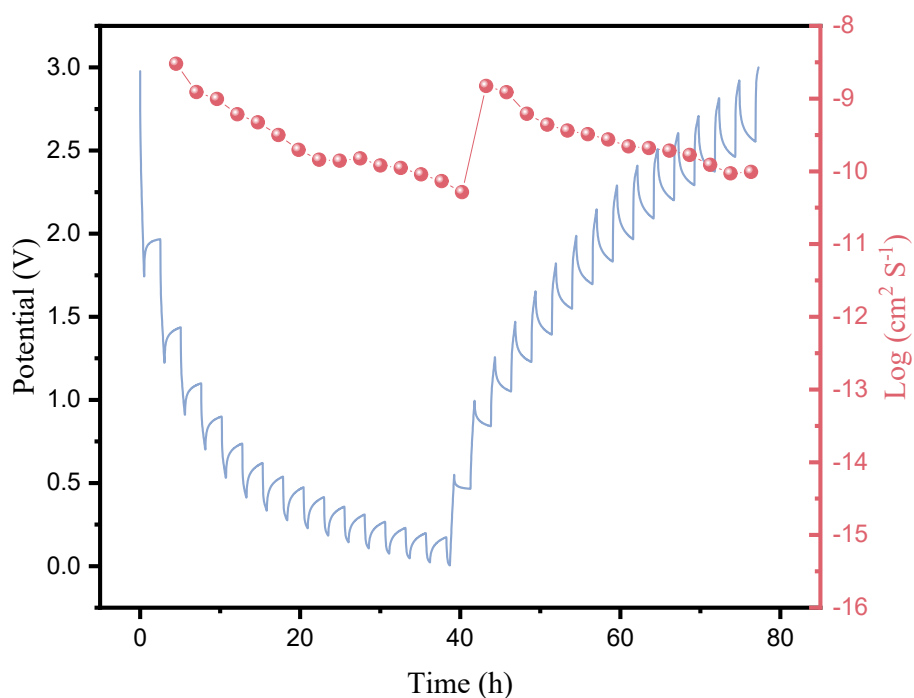


**Fig. S57** GITT curve and diffusion coefficient of the COFs@BOA-30 electrode.

## 11. X-ray Photoelectron Spectroscopy (XPS)
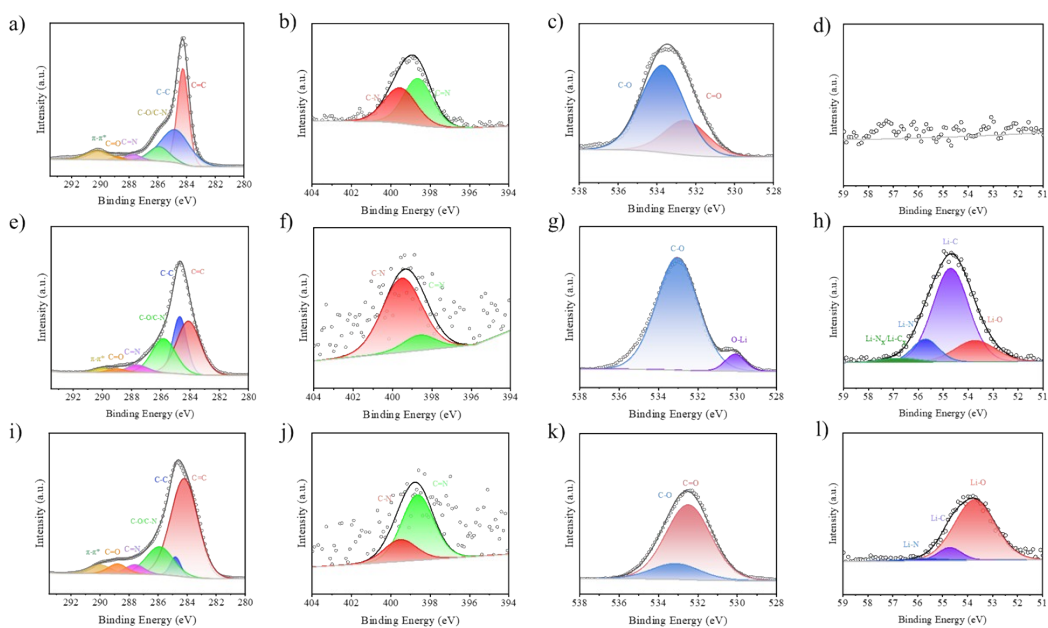
**Fig. S58** XPS spectra of COFs@IM-30: (a-d) XPS spectra of the as-prepared the anode: (a) the C 1s scan; (b) the N 1s scan; (c) the O 1s scan; (d) the Li 1s scan; (e-h) XPS spectra of the lithiation of anode: (e) the C 1s scan; (f) the N 1s scan; (g) the O 1s scan; (h) the Li 1s scan; (i-l) XPS spectra of the delithiation of anode: (i) the C 1s scan; (j) the N 1s scan; (k) the O 1s scan; (l) the Li 1s scan.
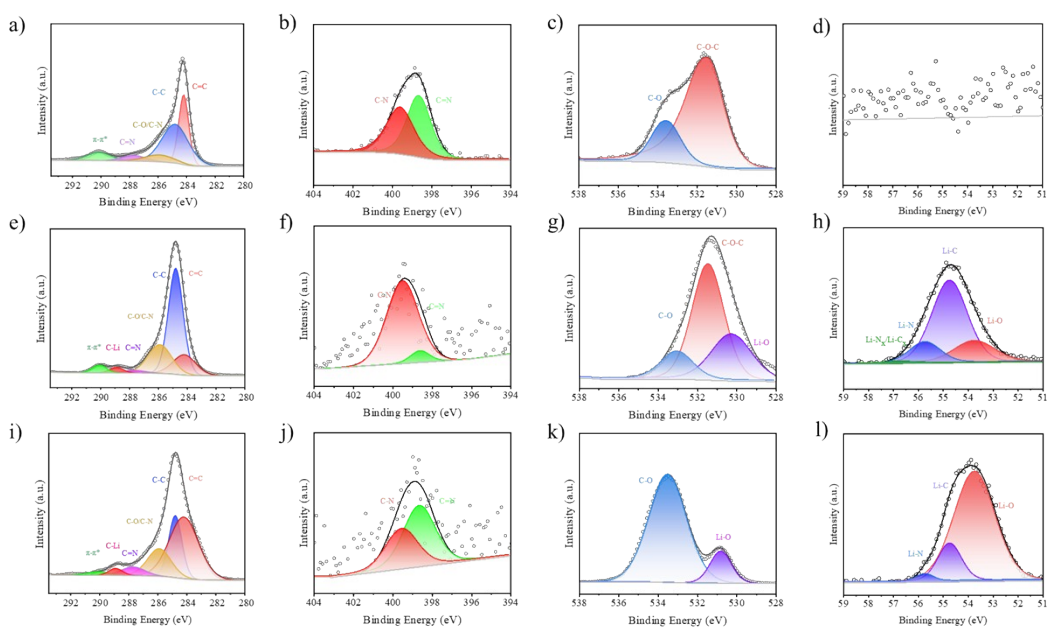


**Fig. S59** XPS spectra of COFs@BOA-30: (a-d) XPS spectra of the as-prepared the

anode: (a) the C 1s scan; (b) the N 1s scan; (c) the O 1s scan; (d) the Li 1s scan; (e-h)

XPS spectra of the lithiation of anode: (e) the C 1s scan; (f) the N 1s scan; (g) the O 1s

scan; (h) the Li 1s scan; (i-l) XPS spectra of the delithiation of anode: (i) the C 1s scan;

(j) the N 1s scan; (k) the O 1s scan; (l) the Li 1s scan.

## 12. Proposed reversible electrochemical redox mechanism
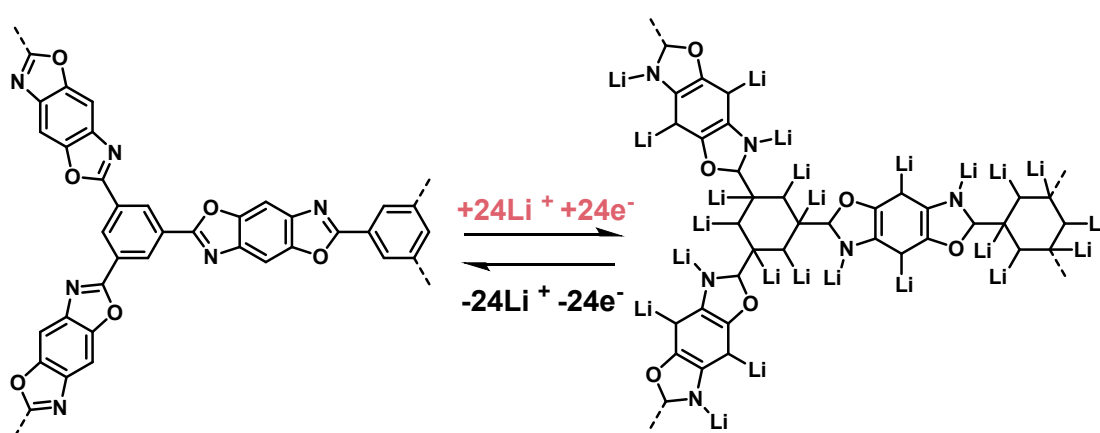


**Fig. S60** Structural evolution of COFs@BOA during the lithiation/delithiation

procedure.

# 13. Band structures
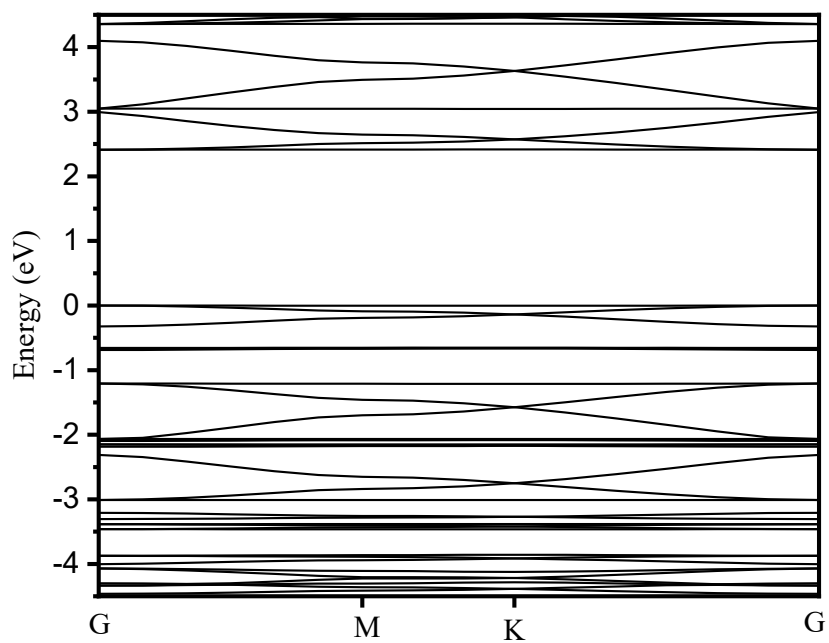


**Fig. S61** Band structures of the COFs@BOA
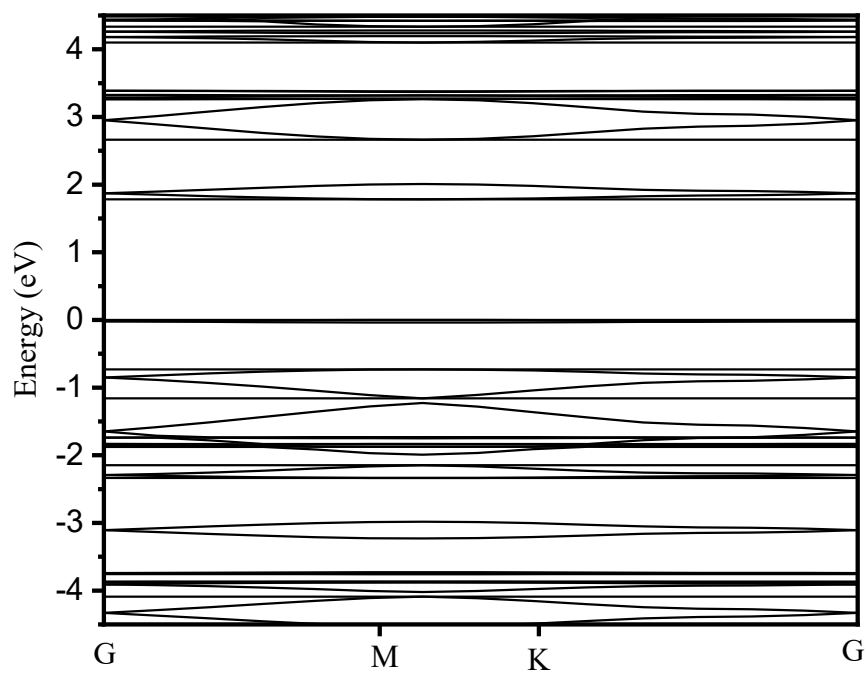
**Fig. S62** Band structures of the COFs@IM

## 14. Comparison of the electrochemical performances

**Table S3** Comparison of the electrochemical performances of the COFs-based carbon materials for the anode of lithium-ion batteries in the literature.

| Abbreviation for COFs-based anode | Capacity/Cycles (mA h g$^{-1}$) | Current density (mA g$^{-1}$) | Voltage range (V) | Ref. |
|---|---|---|---|---|
| **COF@IM-30** | **1100.3/150** | 100 | 0.005-3.0 | **This work** |
| **COFs@BOA-30** | **916.0/150** | 100 | 0.005-3.0 | **This work** |
| DCB-COF-450 | 452/200 | 200 | 0.01-3.0 | [2] |
| PMDA-NiPc | 590/600 | 100 | 0.1-3.0 | [3] |
| PMDA-NiPc-G | 1290/600 | 100 | 0.1-3.0 | [3] |
| COF@CNTs | 1021/500 | 100 | 0.005-3.0 | [4] |
| E-TFPB-COF | 968/300 | 100 | 0.005-3.0 | [5] |
| Tp-Ta-COF | 418/100 | 200 | 0.01-3.0 | [6] |
| COF@CNT-2 | 570/100 | 100 | 0.01-3.0 | [7] |
| Tp-OH-COF | 720/- | 100 | 0-3.0 | [8] |
| Tp-Azo-COF | 513/100 | 100 | 0.01-3.0 | [9] |
| Cz-COF-1 | 236/400 | 200 | 0-3.0 | [10] |
| N2-COF | 600/500 | 1000 | 0.05-3.0 | [11] |
| N3-COF | 593/500 | 1000 | 0.05-3.0 | [11] |
| TThPP | 381/2000 | 1000 | 0.005-3.0 | [12] |

**Table S4** Comparison of GITT of the COFs-based carbon materials for the anode of lithium-ion batteries in the literature.

| Abbreviation for COFs-based anode | GITT (cm$^2$ S$^{-1}$) | Ref. |
|---|---|---|
| **COF@IM-30** | $5.74 \times 10^{-11}$ to $3.63 \times 10^{-9}$ | **This work** |
| **COFs@BOA-30** | $5.16 \times 10^{-11}$ to $3.01 \times 10^{-9}$ | **This work** |
| E-FCTF | $2.36 \times 10^{-10}$ to $7.88 \times 10^{-9}$ | [13] |
| FCTF | $3.15 \times 10^{-12}$ to $7.27 \times 10^{-11}$ | [13] |
| E-CTF | $2.43 \times 10^{-11}$ to $5.09 \times 10^{-10}$ | [13] |
| rCTF | $8.82 \times 10^{-12}$ to $7.00 \times 10^{-11}$ | [14] |
| g-C3N4 | $10^{-15}$-$10^{-17}$ | [15] |
| Azo-CHF | $10^{-11}$ to $10^{-7}$ | [15] |
| Co-COF | $1.96 \times 10^{-14}$ to $5.79 \times 10^{-13}$ | [16] |
| S-CTF-Et | about $10^{-8}$ | [17] |
| S-CTF-Me | $10^{-8}$ to $10^{-15}$ | [17] |

# 15. Atomistic coordinates of COFs@IM and COFs@BOA

**Table S5** Fractional atomic coordinates for the structure of AA stacking of COFs@BOA

| P6/M hexagonal | | | |
|---|---|---|---|
| a = b = 20.9018 Å, c = 3.4460 Å | | | |
| α=β= 90°, γ= 120° | | | |
| Atom | x/a | y/b | z/c |
| O1 | 0.51803 | 0.38111 | 0 |
| C2 | 0.58938 | 0.2972 | 0 |
| C3 | 0.62572 | 0.25613 | 0 |
| C4 | 0.59444 | 0.41834 | 0 |
| N5 | 0.62588 | 0.49014 | 0 |
| C6 | 0.43093 | 0.42819 | 0 |
| C7 | 0.50065 | 0.43629 | 0 |
| C8 | 0.5681 | 0.50444 | 0 |
| H9 | 0.52934 | 0.26826 | 0 |
| H10 | 0.38011 | 0.37513 | 0 |

**Table S6** Fractional atomic coordinates for the structure of AA stacking of COFs@IM

| P6/M hexagonal | | | |
|---|---|---|---|
| a = b = 22.9668 Å, c = 3.4304 Å | | | |
| α=β= 90°, γ= 120° | | | |
| Atom | x/a | y/b | z/c |
| C1 | 0.40501 | 0.54915 | 0.5 |
| C2 | 0.45649 | 0.52766 | 0.5 |
| C3 | 0.43094 | 0.45786 | 0.5 |
| C4 | 0.47235 | 0.42939 | 0.5 |
| O5 | 0.56132 | 0.64103 | 0.5 |
| N6 | 0.42028 | 0.61165 | 0.5 |
| C7 | 0.37503 | 0.63791 | 0.5 |
| C8 | 0.40323 | 0.7078 | 0.5 |
| H9 | 0.35292 | 0.50992 | 0.5 |
| H10 | 0.37702 | 0.42394 | 0.5 |
| H11 | 0.53395 | 0.66396 | 0.5 |
| H12 | 0.45735 | 0.73816 | 0.5 |

# Reference

1.    Elton, L. R. B.; Jackson, D. F., X-Ray Diffraction and the Bragg Law. *Am. J. Phys.* **1966,** *34* (11), 1036-1038.

2.    Cai, Y.-Q.; Gong, Z.-T.; Rong, Q.; Liu, J.-M.; Yao, L.-F.; Cheng, F.-X.; Liu, J.-J.; Xia, S.-B.; Guo,

H., Improved and stable triazine-based covalent organic framework for lithium storage. *Appl. Surf. Sci.* **2022,** *594*, 153481.

3. Zhao, J.; Zhou, M.; Chen, J.; Wang, L.; Zhang, Q.; Zhong, S.; Xie, H.; Li, Y., Two Birds One Stone: Graphene Assisted Reaction Kinetics and Ionic Conductivity in Phthalocyanine-Based Covalent Organic Framework Anodes for Lithium-ion Batteries. *Small* **2023,** *19* (44), e2303353.

4. Lei, Z.; Yang, Q.; Xu, Y.; Guo, S.; Sun, W.; Liu, H.; Lv, L. P.; Zhang, Y.; Wang, Y., Boosting lithium storage in covalent organic framework via activation of 14-electron redox chemistry. *Nat. Commun.* **2018,** *9* (1), 576.

5. Chen, X.; Li, Y.; Wang, L.; Xu, Y.; Nie, A.; Li, Q.; Wu, F.; Sun, W.; Zhang, X.; Vajtai, R.; Ajayan, P. M.; Chen, L.; Wang, Y., High-Lithium-Affinity Chemically Exfoliated 2D Covalent Organic Frameworks. *Adv. Mater. (Weinheim, Ger.)* **2019,** *31* (29), e1901640.

6. Zhao, G.; Sun, Y.; Yang, Y.; Zhang, C.; An, Q.; Guo, H., Molecular engineering regulation redox-dual-active-center covalent organic frameworks-based anode for high-performance Li storage. *EcoMat* **2022,** *4* (6), e12221.

7. Yang, X.; Lin, C.; Han, D.; Li, G.; Huang, C.; Liu, J.; Wu, X.; Zhai, L.; Mi, L., In situ construction of redox-active covalent organic frameworks/carbon nanotube composites as anodes for lithium-ion batteries. *J. Mater. Chem. A* **2022,** *10* (8), 3989-3995.

8. Zhai, L.; Li, G.; Yang, X.; Park, S.; Han, D.; Mi, L.; Wang, Y.; Li, Z.; Lee, S. Y., 30 Li+-Accommodating Covalent Organic Frameworks as Ultralong Cyclable High-Capacity Li-Ion Battery Electrodes. *Adv. Funct. Mater.* **2021,** *32* (9), 2108798.

9. Zhao, G.; Zhang, Y.; Gao, Z.; Li, H.; Liu, S.; Cai, S.; Yang, X.; Guo, H.; Sun, X., Dual Active Site of the Azo and Carbonyl-Modified Covalent Organic Framework for High-Performance Li Storage. *ACS Energy Lett.* **2020,** *5* (4), 1022-1031.

10. Feng, S.; Xu, H.; Zhang, C.; Chen, Y.; Zeng, J.; Jiang, D.; Jiang, J. X., Bicarbazole-based redox-active covalent organic frameworks for ultrahigh-performance energy storage. *Chem. Commun. (Cambridge, U. K.)* **2017,** *53* (82), 11334-11337.

11. Bai, L.; Gao, Q.; Zhao, Y., Two fully conjugated covalent organic frameworks as anode materials for lithium ion batteries. *J. Mater. Chem. A* **2016,** *4* (37), 14106-14110.

12. Yang, H.; Zhang, S.; Han, L.; Zhang, Z.; Xue, Z.; Gao, J.; Li, Y.; Huang, C.; Yi, Y.; Liu, H.; Li, Y., High Conductive Two-Dimensional Covalent Organic Framework for Lithium Storage with Large Capacity. *ACS Appl. Mater. Interfaces* **2016,** *8* (8), 5366-75.

13. Zhang, H.; Sun, W.; Chen, X.; Wang, Y., Few-Layered Fluorinated Triazine-Based Covalent Organic Nanosheets for High-Performance Alkali Organic Batteries. *ACS Nano* **2019,** *13* (12), 14252-14261.

14. Buyukcakir, O.; Ryu, J.; Joo, S. H.; Kang, J.; Yuksel, R.; Lee, J.; Jiang, Y.; Choi, S.; Lee, S. H.; Kwak, S. K.; Park, S.; Ruoff, R. S., Lithium Accommodation in a Redox-Active Covalent Triazine Framework for High Areal Capacity and Fast-Charging Lithium-Ion Batteries. *Adv. Funct. Mater.* **2020,** *30* (36).

15. Yu, Y.; Jin, Q.; Zhu, D.; Ren, Y., Exceptional Lithium-Ion Storage Performance on an Azo-Bridged Covalent Heptazine Framework. *Adv. Funct. Mater.* **2023,** *34* (2), 2308706.

16. Wang, H.; Zou, W.; Liu, C.; Sun, Y.; Xu, Y.; Sun, W.; Wang, Y., β-Ketoenamine-Linked Covalent Organic Framework with Co Intercalation: Improved Lithium-Storage Properties and Mechanism for High-Performance Lithium-Organic Batteries. *Batteries Supercaps* **2023,** *6* (3).

17. Geng, Q.; Xu, Z.; Wang, J.; Song, C.; Wu, Y.; Wang, Y., Tailoring covalent triazine frameworks

anode for superior Lithium-ion storage via thioether engineering. *Chem. Eng. J.* **2023,** *469*, 143941.